EROSION-CORROSION DEGRADATION OF ADDITIVELY MANUFACTURED METALS

MECH5080M Team Project – Individual Report

EROSION-CORROSION DEGRADATION OF ADDITIVELY MANUFACTURED METALS

Author: Robert Patton (201326508)

Supervisor: Joshua Owen

Industrial Mentor: Sulzer Pumps Ltd.

Examiner: Richard Barker

Date: 30/04/2024

Contents

Abstract

The erosion-corrosion performance of conventionally and additively manufactured (AM) Inconel® has been investigated through the development of a combined analytical and experimental methodology. Current erosion-corrosion models cannot be used to accurately predict wear in complex systems. Informed by the method proposed by Gnanavelu et al. [1], results from a $10ms^{-1}$ and $20ms^{-1}$ average flow velocity computational model of a submerged impinging jet apparatus were synthesised with corresponding wear scar profiles to produce several “wear maps” that were used to predict wear in new flow environments. The method was applied to an AM material for the first time, in both erosion and erosion-corrosion conditions.

Sulzer Ltd, the project sponsor, produce pumping machinery that operate in erodent rich, corrosive environments. Aqueous sodium chloride and sand were selected as the corrosive species and erodent respectively, to replicate the conditions of interest to Sulzer.

The maps accurately predicted the wear scar profiles of the $10ms^{-1}$ and $20ms^{-1}$ flow cases, with a mean average squared error (MASE) of 26% but were unable to predict wear for an intermediate $15ms^{-1}$ flow velocity, with a MASE of 106%. This is thought to be associated with the larger $5ms^{-1}$ velocity delta between the input data, compared to the $2.5ms^{-1}$ delta chosen by Gnanavelu et al. [1]. This highlights that a limitation of the wear mapping technique: predictions are limited by the linear interpolation between the input data, and therefore the map must be calibrated with data close to the flow regime of interest to be accurate. This is a key finding for those who may wish to leverage this technique to make accurate erosion-corrosion predictions, such as Sulzer.

Appendix B

The work presented in the main report was extended through the development of a novel machine learning model. The wear map method is material and condition specific, and these limitations are overcome by the ML model developed, which accurately predicts the erosion expected at $15ms^{-1}$, with a MASE of 34%. In theory the model is material and condition specific, though further work needs to be done to evaluate the extent to which it can operate successfully outside of its training space. This would require further experimental testing with new materials and conditions.

Appendix B is not expected to be reviewed or assessed.

Chapter 1 - Introduction

This individual report forms part of a larger team investigation into the erosion and corrosion behaviour of a variety of materials and manufacturing methods and will focus primarily on the development of a combined analytical and experimental method to improve material degradation understanding and predictions.

1.1. Introduction

Wear of fluid handling components is accelerated when flows are corrosive and mass laden [1,2]. This combined mechanical and chemical degradation rapidly reduces part lifetimes, increasing the risk of leaks and system failure [1]. This is a significant challenge faced by industries where safe and economical transport of slurries is required, such as found in geothermal, renewable energy and oil and gas systems [3].

Sulzer, a company that design and manufacture fluid and chemical processing equipment, are looking to improve the performance of their products by increasing their efficiency and sustainability. As local wear rates across complex systems are difficult to predict analytically, critical parts are typically manufactured from corrosion resistant alloys or given protective coatings that increase their lifespan. However, these solutions are expensive and restrict design freedom [4].

Two technologies exist that could be leveraged to advance both the performance of parts operating in these harsh environments, and better predict where degradation will occur, so that these expensive countermeasures can be used more efficiently: Additive manufacturing (AM) [5] and Computational Fluid Dynamics (CFD) [1,2,6,7].

AM encompasses a suite of manufacturing processes where parts are produced layer by layer, instead of through a conventional subtractive (machining) or formative (casting, moulding) processes. AM also affords greater design freedom and can be used to produce materials with enhanced erosion and corrosion resistance [5]. Therefore, parts could be produced with greater mechanical and corrosive resistance that also, through more complex geometry, increase the global system efficiency, such as in pumps and agitation equipment. Sulzer now routinely use AM methods to repair conventionally manufactured parts, and further research to classify the behaviour of these materials would give increased confidence in their widespread adoption.

CFD, through rapid improvements in computational power over the last two decades [8], has become a staple tool to predict flows in complex systems [9]. Fluid flow models can be extended through particle and species transport simulations to predict erosion and corrosion wear in standard test scenarios, such as submerged

impinging jets (SIJ) [1–3,6,7]. However, these models struggle to accurately predict wear in complex systems [3]; further research and development is needed.

A combined analytical and experimental method developed by Gnavelu et al. [1], has been proven to improve the accuracy of erosion wear predictions through the development of a wear map, with a number of similar strategies developed recently [3]. These maps, when combined with a CFD simulation, can then be used to predict performance of a sample in a new scenario. This is a significant step towards predicting the wear in complex systems found in industry, and further research and extension of this method would allow companies such as Sulzer to better predict how new system configurations will behave, without having to rely on expensive real-world testing.

A limitation of this method though is that the wear map generated is material and erodent specific, with only conventional materials and erosion only conditions investigated. This individual report will focus on producing wear maps for conventional and additively manufactured materials in erosion and erosion-corrosion conditions.

As with CFD, improvements in computational power have allowed machine learning (ML) algorithms to develop into general purpose tools that are, for example, now leveraged to improve failure predictions and industrial system maintenance [10]. A stretch objective of this project will be to investigate the possibility of extending the method developed by Gnanavelu et al. to improve wear predictions more generally.

1.2. Individual Project Aim

Develop a Computational Fluid Dynamics model of a Submerged Impinging Jet and combine the results with experimental data to evaluate and make erosion, corrosion, and erosion-corrosion comparisons and performance predictions of conventionally and additively manufactured corrosion resistant steels.

1.3. Individual Objectives

- Develop a CFD and particle tracing model of the experimental SIJ setup using the software package COMSOL, validating results with comparisons to experimental and analytical data gathered via. wear scar analysis of samples.
- Combine CFD results of 10m/s and 20m/s flow velocities with corresponding experimental data to produce wear maps, validating results through predictions of wear performance of 15m/s flow velocity.
- Compare wear map predictions to conventional erosion and corrosion models.
- **Stretch:** Extend the wear map method by producing a ML model, assessing the accuracy of the predictions against the wear map and experimental wear data.

Chapter 2 - Literature Review

2.1. Introduction

Advancing understanding of erosion and corrosion presents both great economic and environmental opportunities. A recent survey conducted by the National Association of Corrosion Engineers (NACE) found the industry cost of corrosion to be $401 Billion US Dollars in Europe, of a global $2.5 Trillion annual expenditure [4]. The Oil and Gas, Pipelines and Water industries have driven much of the research in this field. In addition to reducing costs, preventing high profile failures has also motivated progress in corrosion management [4]. Reducing failure risk improves staff safety while also protecting the environment and company reputation.

Despite the significant incentives, a universal method for predicting local erosion and corrosion wear remains elusive. Instead, research is limited to producing qualitative material rankings, as opposed to quantitative model predictions [1]. A review of the field in 1997 by Hsu et al., investigated two hundred theoretically and empirically based models [11]. The authors concluded that none could sufficiently predict wear from material properties and contact information alone, though discussed methods such as wear mapping as areas of potential improvement [11].

A more recent review of developments in erosion-corrosion, published in 2017 by Burson-Thomas and Wood, again states that no general theory to predict wear has been found [3]. In addition to the complexity of the phenomenon, the authors postulate that the domination of application-specific studies, as opposed to the search for a general theory, has slowed progress towards a universal, non-material-specific method. They highlight CFD and erosion-corrosion mapping to develop our understanding, with research proving that CFD, in combination with experimental data, can accurately predict erosion and corrosion wear [1,3,6,7,12]. However, these models are limited as they require several empirical factors to be adjusted according to specific materials and scenarios in order to provide accurate results.

In addition to improvements in wear prediction, new AM materials could improve the performance and longevity of fluid handling systems. AM materials offer increased design freedom and better erosion and corrosion performance over conventional materials [5]. The adoption of these materials offers an exciting opportunity to improve corrosion management industry, as demonstrated by Sulzer. However, research is limited with erosion-corrosion performance of AM materials not yet fully understood [5].

This paper will further investigate the development of CFD and wear maps to predict the erosion and erosion-corrosion performance of conventional and new AM materials, for which this technique has not been applied.

2.2. Corrosion

Corrosion is the deterioration of a surface due to a physiochemical interaction between a material and chemical species in the environment. Corrosion can be subdivided into electrochemical, chemical, biological, and mechanically assisted modes, such as pure erosion, and erosion-corrosion [13]. Informed by Sulzer, this report will focus on the pure erosion, and erosion-corrosion of steels in aqueous sodium chloride solutions.

The chemical corrosion of steel in sodium chloride solutions, where refined metal is reverted to its more stable energy state (Fe3+) by an oxidation reduction reaction; this is investigated in detail in the team report. Though some mass transfer coefficient (MTFC) data, is adopted from Tsun Li, [14], and discussed in Appendix B.

As the corrosion process is extremely complex, basic flow parameters such as Reynolds number, shear stress and turbulent intensity cannot be used to accurately predict local wear rates [7]. However, recent studies have shown that corrosion rates can be accurately predicted in complex systems by coupling CFD simulations with corrosion theory [15], such as the H+ ion transfer model described by Owen [7]. The author found that for an expansion pipe geometry, the corrosion rate predicted correlated well with experimental data. This is important as the local corrosion rate can be predicted, as opposed to just the calculation of a maximum corrosion expected.

A limitation of this method is the need for a high-fidelity K-W SST transfer model, and the dependence of the results on the Turbulent Schmidt number [7]. The SST model is more computationally expensive as it requires a more refined mesh (lower y+ value) than other models. The Turbulent Schmidt number can be found through experimental investigation, though this can be expensive and time consuming.

2.3. Erosion

Erosion, as caused by individual abrasive particles, was first described by Finnie as the wear of a material that results from the attack on a solid surface by particles entrained in a fluid, and that to understand erosion, the motion of particles in fluid streams and the amount of material removed by an interaction must be determined [16]. In this early work, the Finnie describes how fluid mechanics could be combined with an understanding of the cutting action of hard particles to describe this phenomenon. In a later work (1971), Finnie states 10 parameters that influence ductile erosion, with the most influential of these as the impinging particles angle, rotation, velocity, and size [17]. These are described in Figure 1, adopted from this paper [16].

Over 200 models of erosion have since been proposed, though no general theory has been agreed upon, as found in a systematic review by Hsu et al. [11]. Hsu

et al. identified 32 distinct parameters across 28 models of merit, which include those stated by Finnie, along with application and material specific empirical quantities, such as hardness, fracture toughness and erosion resistance. These parameters have been proven to have a significant impact on results [12], and so need to be accurately defined for a specific material and condition before models can be applied, which is often time consuming and expensive.

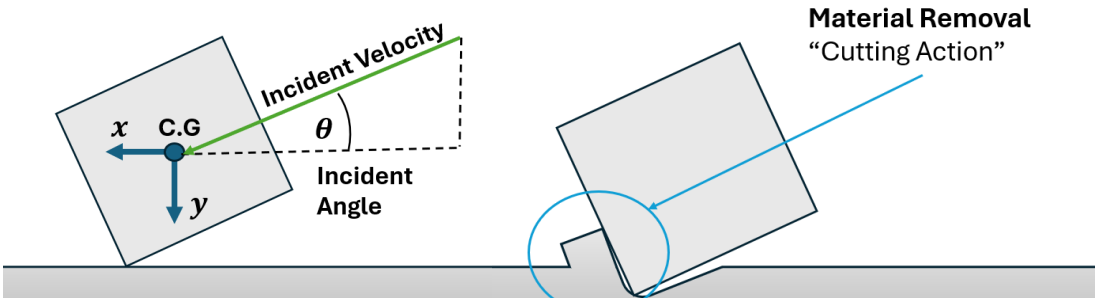

Figure 1 - Cutting action model for an abrasive particle incident on a surface, adopted from [16].

2.4. Erosion-Corrosion

Erosion-corrosion is a complex mechanism where material wear results due to both individual erosion and corrosion, and a combined erosion-corrosion phenomenon that accelerates material removal [2,3]. The erosion-corrosion rate is described by Owen as the sum of the pure erosion (E) and corrosion (C) components, plus the sum of the erosion enhanced corrosion (δC_E) and corrosion enhanced erosion (δE_C) – Eq. 1 [2].

$$EC_{TML} = E + C + \delta C_E + \delta E_C \qquad (1)$$

It should be restated that no general theory of Erosion-Corrosion has been agreed upon [3]; however, one likely mechanism of erosion enhanced corrosion is he roughening of the surface sample, which is thought to enhance dissolution rates [2].

Corrosion enhanced erosion can also be significant, with the corrosion of work-hardened layers thought to play a key role. During erosion only, a layer of work hardened material forms that protects softer material. In a corrosive environment, this layer is attacked, and so soft material is continually exposed to particle attacks.

An additional theory for erosion enhanced corrosion is the removal of protective passive or corrosion inhibiting films that are damaged by particle action. Laleh et al. observed that AM 316L steel exhibited weaker repassivation ability than conventionally produced material, thought to be due to the increased porosity of the material [5] - a key consideration for models concerning AM materials.

2.5. CFD, Wear Map Method

Computational Fluid Dynamics (CFD) is routinely used in a variety of engineering fields to study fluid flows from computation of solutions to the inviscid (Eulerian) and viscous

(Navier-Stokes) governing equations [18]. CFD simulations can be extended with various physical models to represent multiphase flows, that may consist of solids, liquids, and gasses [19]. To model erosion, particle tracing techniques can be employed. The LaGrange approach and Eulerian approach are two common methods where particles are modelled as points individually (LaGrange), or as a concentration that moves by diffusion and convection (Eulerian) [20]. Of these, the former is suited to model particles for this study.

Before the advent of CFD, McLaury developed a rigorous process to predict wear rate due to particle impacts, built upon the limited research done at the time. They proposed three stages: modelling the flow, simulating particles, and then inputting the results to an erosion model [21]. This approach was successful, though was limited to specific conditions by empirical constants required by the analytical erosion model.

Gnanavelu et al. showed that this basic procedure could be modified to predict wear in different geometries through the development of a “wear map” that can be used in place of an analytical erosion model [1]. Specifically, “The findings demonstrate that a standard jet impingement test can provide enough data to allow predictions of wear rates within different geometries, which opens up the possibility of predicting (rather than just ranking) material performance in plant equipment.” [1]. In a later comparative study, this method was shown to outperform traditional models across a full range of impingement angles [6], and is cited as a promising area of further research [3]. An example map is available in Appendix A.1 (Figure 14.).

The map is generated from the combination of experimental and CFD impact data in a calibration step. The map is a two-dimensional (2D) surface that can be sampled by CFD data and averaged to predict wear depth. This method benefits from a range of experimental data. A limitation of the wear map is that it is material and erodent specific. An opportunity exists to compare wear maps of multiple materials and to build a non-specific map where material and condition values are inputs - see Appendix B.2.

2.6. Erosion-Corrosion Testing

Submerged Impingement Jets (SIJs) are a suitable choice for erosion-corrosion testing as the constituent erosion, corrosion, and erosion-corrosion contributions (eq.1) can be evaluated using one apparatus; the results can also be compared to previous experiments for validation [2]. In addition, a wide range of impingement angles are generated [1], increasing the calibrated area, and thus the usefulness, of a wear map.

A wear scar is formed on a sample surface after SIJ testing, and to produce a wear map, the scar profile must be measured. Optical Profilers are suitable to extract

topographical data [1,2]. White light interferometry is used to capture a 3D profile with, from which a 2D scar can be extracted with around $\pm 0.02 \mu m$ precision.

2.7. AM Materials

AM materials are produced by layers of material that are deposited sequentially to build up a part, as opposed to a subtractive or formative process. The technology has enjoyed rapid adoption over the last 40 years, summarised in a systematic review by Franco et al. [22]. The authors state the facilitation of complex parts, increased product design freedom and diversity and reduced production complexity as some of the benefits of AM adoption. This evidence is also supported anecdotally by our industry sponsor Sulzer, who are looking to introduce AM manufactured parts later this year.

In addition to these benefits, an investigation by Chao et al revealed 316L Stainless Steel (SS) produced by selective laser melting (an AM process) exhibited enhanced pitting corrosion resistance to a conventional counterpart with comparable grain size and chemical composition [23]. The authors attribute this to a potential reduction in MnS inclusions in the AM material that otherwise harms performance. This view is also shared by Laleh et al. who also found SLM 316L SS to have higher hardness than a conventional specimen [5].

Conventional materials with greater hardness and pitting corrosion resistance usually have greater erosion-corrosion performance, so AM materials would be expected to perform better than conventionally produced materials. However, this was not found by Laleh et al., who observed unexpectedly worse behaviour [5]. They believe this may be due to the weaker repassivation ability of the SLM sample, though note that further work should be done to investigate this.

2.8. Conclusion

This literature review has introduced the principles of erosion, corrosion and erosion-corrosion as they apply to fluid transport systems and has demonstrated the potential economic and socioeconomic opportunities that improving erosion-corrosion wear predictions and understanding present. The development of techniques to predict wear have been discussed, including the wear map method. This is a promising area of research, particularly with exciting new AM materials that warrant further investigation.

Chapter 3 – Methodology

3.1. Experimental Data

Conventional and AM Inconel, a high-performance steel of interest to Sulzer, was selected for this study, from which 18 samples were produced. The materials were tested in erosive (E) and erosion-corrosion (EC) conditions, with sand concentrations of 500 and 1000mgL, and at flow rates of 10, 15 and 20ms^{-1}. This work was conducted by team members Jasper Alderton and Josh Maddison, who discuss this in detail in their individual reports [24], [25], and who have given permission for the experimental data to be adopted. Samples were then scanned and the 2D profiles were extracted.

Unfortunately, the SIJ pump failed before the team could collect repeat results. This reduces the level of confidence in our wear scar profiles, which in turn reduces the confidence in the final wear maps. This is elaborated on further in the discussion.

3.2. Computational Model

The incident angle and velocity of the particles incident on a surface are critical to describing and modelling erosive wear [1,2,6,11,16]. As discussed in the literature review, a computational model can be built to provide this input data.

COMSOL Multiphysics V6.1 was used to develop a model of an impinging jet. An additional advantage of using a SIJ is that an axisymmetric model can be used, which reduces the computational resources required [1,2]. A k-ω turbulent model was used as an approximation to the Reynolds-Averaged-Navier-Stokes (RANS) equations and to solve for the flow. This model was then extended by Tsun Li to predict the mass transfer coefficient at the surface using a k-ω SST model [14], see Appendix B.

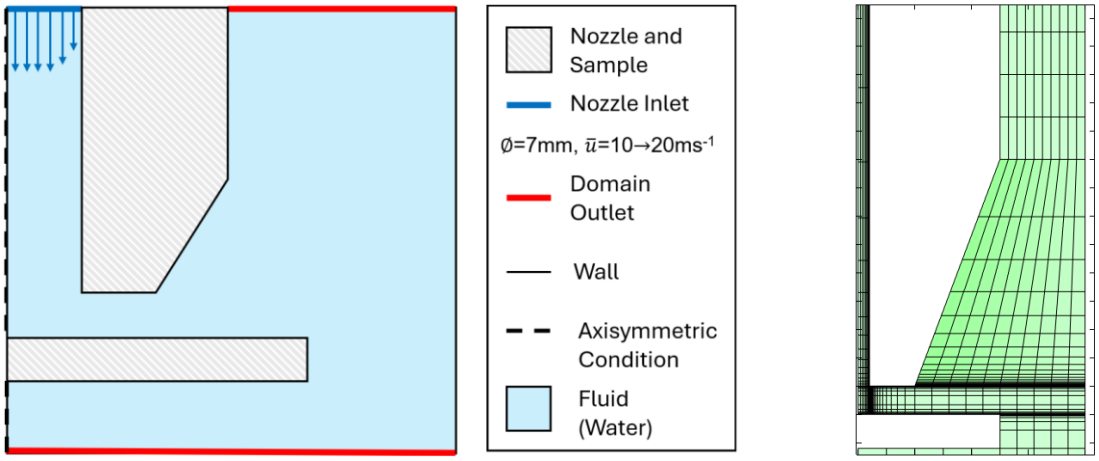

Figure 2 - SIJ Model domain and B.Cs (not to scale). Figure 3 - Meshing Strategy Illustration (to scale).

The model and mesh strategy are shown in Figure 2. An axisymmetric model was used, informed by other studies [1,2], in combination with a structured mesh to reduce computational effort required without a significant accuracy penalty.

Once the flow regime was computed, a time dependant fluid particle tracing model was developed. Equations were added to model the drag, gravity and buoyancy forces the particles are subject to – see eq. 4-7, Appendix A.5.

Once the CFD model was developed, exhaustive mesh convergence and sensitivity testing was conducted, with the grid convergence index (GCI) calculated according to Roache's method, adopted by the ASME [26]. The parameters of interest were the element count, radial domain length, first layer height, time step size, particle count and particle size, selected from a review of previous literature and CFD best practices [1,27]. This testing increases the confidence and credibility of the final model.

Validation and Verification is critical in the development of CFD models [27]. The flow was analytically verified by comparison for the formulation of the shear stress at the sample surface, given by Poreh [28], and compared to the results of a corresponding SIJ model produced by Owen [2]. Validation of the flow in an SIJ and the particle tracing results is challenging [2] as it is difficult to measure the incident velocity and angle of particles in these conditions. Instead, secondary results are computed which can be validated against corresponding experimental data [1,2].

3.3. Wear Map Construction

A wear map, first proposed by Gnanavelu et al. [1], is generated by combining the incident velocity and angle data across a sample surface with the corresponding wear depth at that radial distance, obtained from a wear scar profile. This data was collated using MATLAB, and the function "`interp2`" was used to perform bilinear interpolation over a fixed grid of input velocities and angles, producing a 2D wear map.

The method was validated by first modifying the computational model to represent the geometry and flow velocities (Ø=7mm, $\bar{u}$=5ms^{-1}, $\bar{u}$=10ms^{-1}) used by Gnanavelu et al., adopting the wear profile presented, and then comparing the computed maps [1]. The map was then validated by predicting the wear expected, W^{Map}, with the wear measured, $W^{Measured}$, for a 7.5ms^{-1} average flow velocity, $\bar{u}$.

Once this was completed, material and condition specific wear maps were developed from our final 10ms^{-1} and 20ms^{-1} SIJ simulation data and wear profiles. The maps were verified by comparing the actual and predicted wear at a 15ms^{-1} flow velocity, quantified by calculating the root mean squared error (RMSE), and the mean absolute scaled error (MASE) defined by Hyndman [29] – see eq. 2,3. The MASE is advantageous, compared to the RMSE, as it can be used with data of different scales, data close to zero (as found just beyond the wear scar) and it is easy to interpret [29].

$$RMSE = \sqrt{\frac{1}{N}\sum_{i=1}^{n}(W_i^{Map} - W_i^{Measured})^2} \quad (2) \qquad MASE = \frac{\frac{1}{N}\sum_{i=1}^{n}\left|W_i^{Map} - W_i^{Measured}\right|}{\frac{1}{N}\sum_{i=1}^{n}(W_i^{Map} - \overline{W^{Map}})} \quad (3)$$

Chapter 4 – Results

4.1. Computational Model Results

A high quality, fully structured mesh was developed with geometry of the corresponding experimental apparatus. Full details are available in Appendix A.5.

To validate the model, it was modified slightly to match the Poreh geometry [28], with a nozzle diameter to nozzle height ratio of 2, to allow the shear stress precited to be verified, shown in Figure 4. An initial convergence test was then performed to ensure this result was accurate, shown in Figure 4.

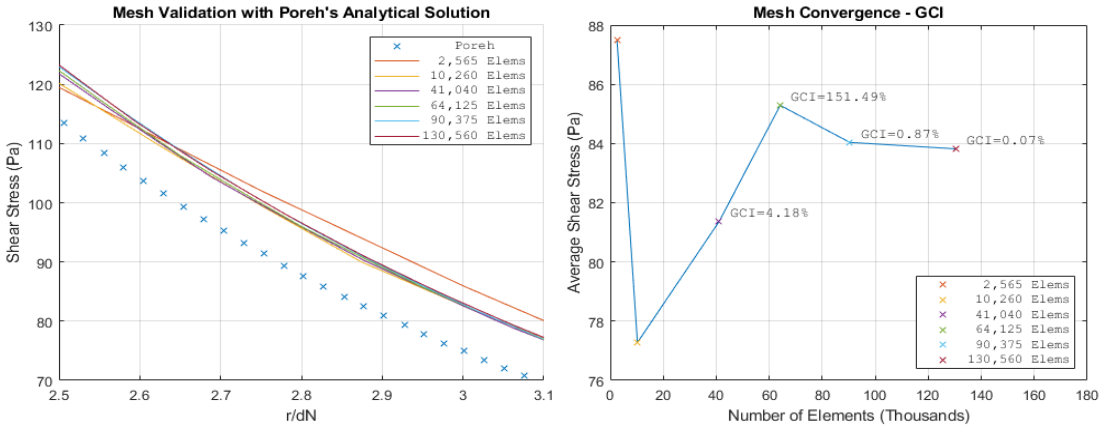

Figure 4 – Validation with data from Poreh [28]. Figure 5 – Mesh convergence results (GCI FS=1.25).

The GCI was calculated, and a mesh with 64,125 total elements was selected. This is as further refinement only gives a GCI of <1%. Full results in Appendix A, (Table 2). Results for the sensitivity study conducted are given in Table 1.

Table 1 – Sensitivity Testing Results. Final value selected given with the GCI indicating the sensitivity.

	Variable Values		Convergence (GCI) at final value			
Model Variable	Range Tested	Final	Impact Velocity	Impact Angle	Shear Stress	Erosion Rate
Geometry Radial Distance (mm)	40, 60, 80 from centre	40	0.000%	0.060%		
First Layer Height (mm)	20e-3→0.4e-3 [y+ 31→0.62]	1.6e-3 [y+ 1.24]	0.015%	0.008%	0.06%	
Time Step Size (s)	0.001→5e-6	5e-5	0.025%	1.330%		
Particle Count	50→10,000	5,000	0.230%	0.002%		0%

The final parameter values were selected as refining the model further has a negligible effect on the final results. The effect of Particle Size was also investigated with results available in Appendix A.2., along with the y+ distribution at the surface. A particle size of 250um was selected as it is the average of the actual particle size.

A convergence study for the final model geometry and parameters is given in Appendix A, (Table 3). A final 67,840 element mesh was selected as further refinement led to a GCI of less than <1% for all results of interest.

4.1.1. Simulation Results

Flow regime and particle tracing results were obtained for a flow velocity of 20ms^{-1}, 10ms^{-1}, and 15ms^{-1}, shown in Figure 6 and Figure 28. For additional plots, including the y+ distribution at the sample surface ($\overline{y^+} \cong 3.1$), see Appendix A.3.

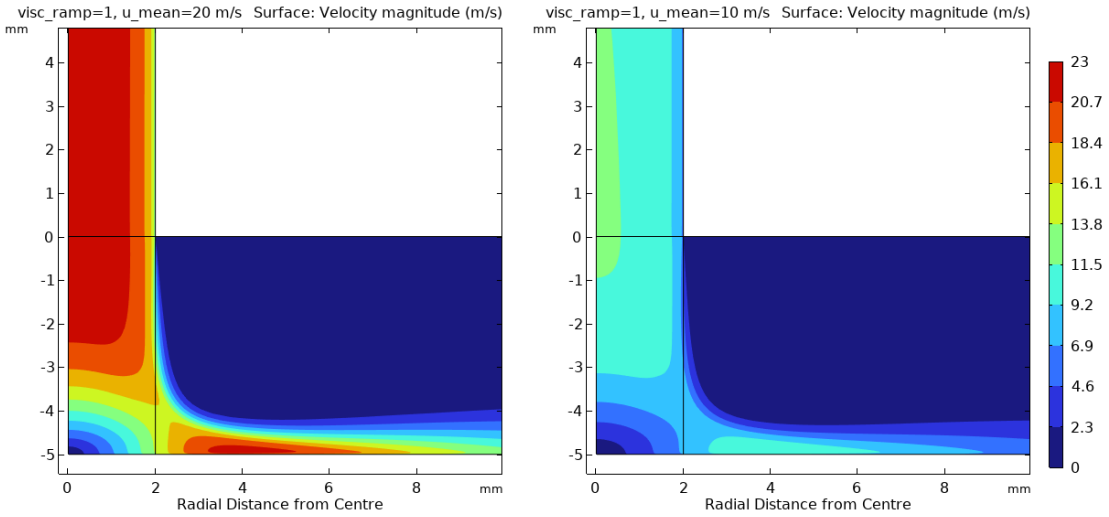

Figure 6, Figure 7 – CFD Flow Results (20ms^{-1},10ms^{-1}), coloured by velocity magnitude in discrete bands.

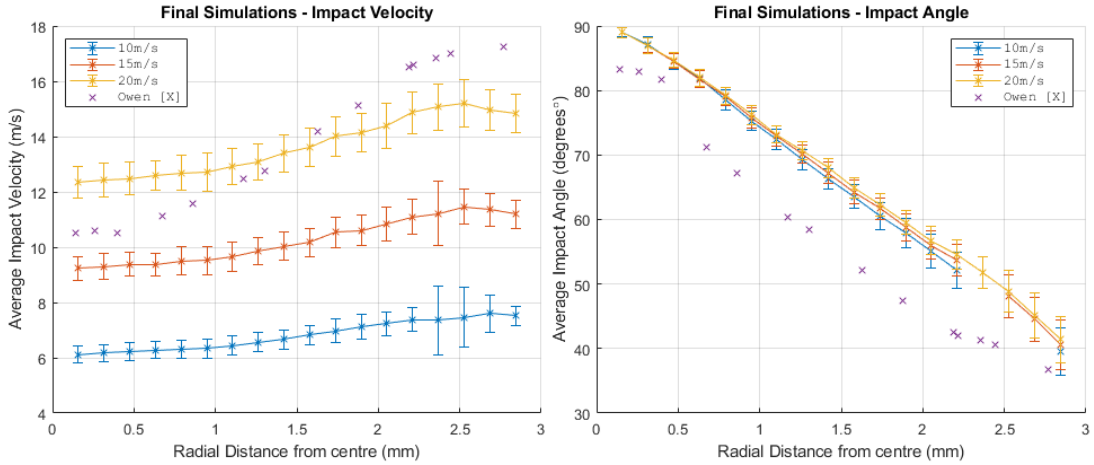

Figure 8, Figure 9 – Averaged Impact Velocity and Angle at different flow velocities. Raw particle data (5000 particles simulated) is available in Appendix A. Vertical Error bars show ± one standard deviation.

The flow regime is comparable to similar SIJ models [1,2,6], with a stagnation point observed. The particle velocity and angle differ from the data provided by Owen [2].

4.2. Wear Mapping

As discussed in the methodology, the MATLAB code to generate the wear maps was validated by recreating Gnanavelu et al.'s wear map [1]. The input data and map produced are available in Appendix A.1. The map performed well, as found by Gnanavelu et al., with an average MASE of 6.27% for the input data ($\bar{u} = 5,\ 10ms^{-1}$) and a MASE of 16.7% for the 7.5ms^{-1} wear profile prediction.

After the erosion-corrosion testing was conducted, the samples provided by the experimental team [24,25] were analysed with a Bruker NPFLEX to extract wear

profiles. These were centred, averaged, and half profiles are given in Figure 10, Figure 11 – Processed wear profiles for the conventional and PBF materials for all conditions.

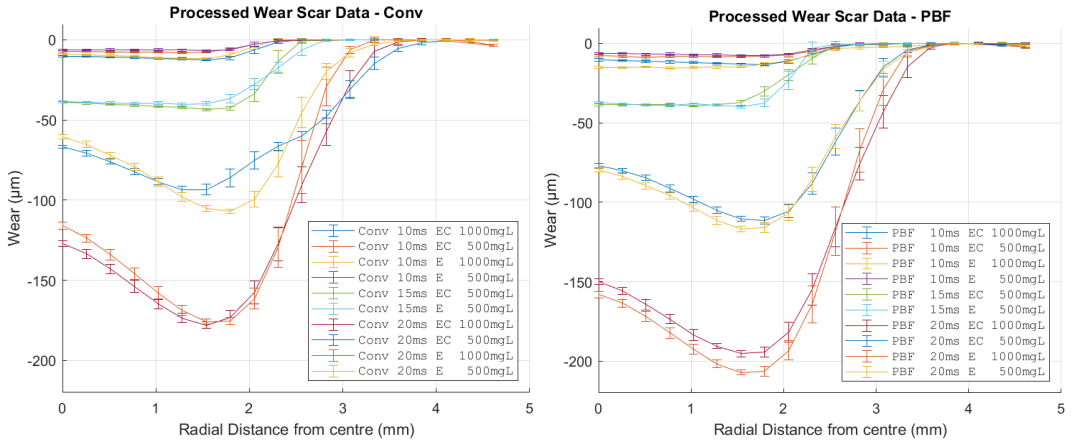

Figure 10, Figure 11 – Processed wear profiles for the conventional and PBF materials for all conditions.

4.2.1. Wear Maps

The profiles were combined with the experimental data to give the maps in Figure 12.

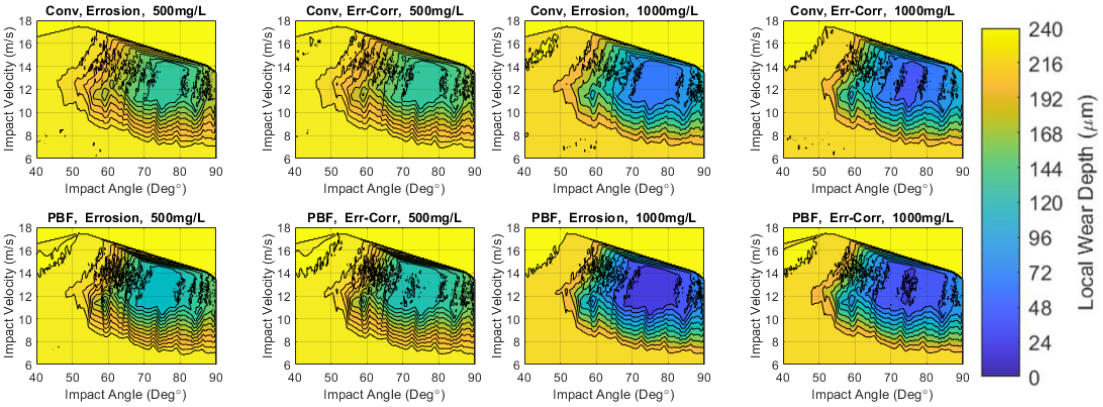

Figure 12 – Final wear maps generated. Full resolution version available in Figure 37.

The wear profiles predicted using the maps in Figure 12 were compared with the measured profiles at 15ms^{-1}, and the MASE was calculated, given in Figure 13.

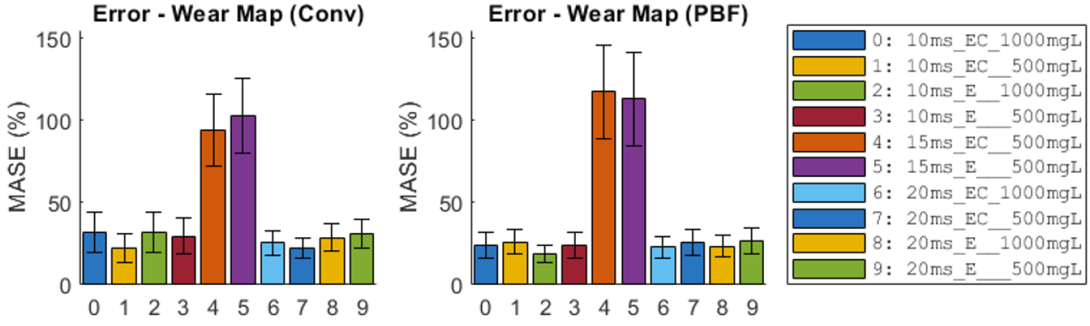

Figure 13 - Wear Map validation, MASE calculated. Error bars show ± 1stdev (error propagation).

Unlike for Gnanavelu, the wear maps were unable to accurately predict the measured wear profiles at 15m/s. See Appendix A.5. for wear maps built with 15m/s data.

Chapter 5 – Discussion

5.1. Computational Model

A computational model with geometry of the corresponding SIJ apparatus was developed, represented by a fully structured mesh with excellent quality (minimum 0.77, average 0.98). This is an advantage over similar SIJ CFD models that use unstructured triangular elements, as a structured mesh require less computational resources, and accuracy is improved by a low skewness [27]. This could contribute to the improvement in the shear stress predicted, which a 4% improvement compared to a similar k-ω model [2], and only 9.3% greater than expected analytically [28].

Comprehensive mesh convergence and sensitivity testing was conducted which has increased the credibility of the model. A rigorous factor of safety of 1.25 was selected when computing the GCI values, increasing the confidence in the final model parameters selected. The results are also comparable to those found by Gnanavelu et al., who developed a model using ANSYS [1], reducing the likelihood of a coding error.

Particle size was found to have the greatest influence on the computed incident angle and velocities (Fig. 20, 21). Unlike the other parameters interrogated by the sensitivity study, the results did not converge, so a value of 250μm was selected as this is the average particle diameter of the erodent used in the experimental testing. It is key to note that the erodent used does not exclusively consist of 250μm diameter sand, and instead the size is expected to follow a normal distribution around this mean value. Though computationally expensive, results could be improved upon in future by combining the results from subsequent simulations according to this distribution.

However, the final incident angle and velocity results do not agree with those computed by Owen [2], as shown in Figure 8. This is most likely as Owen's results were calculated by a previous version of COMSOL, and the simulation was initialised with water at 60 degC, as opposed to 21 degC. As it is difficult to validate particle incident angles and velocities [2], it is difficult to prove if these results are anomalous, and this is one of the most significant flaws with this approach. Instead, secondary results such as erosion rates are calculated and compared to experimental results. The erosion depth predicted by the Finnie model was calculated (Figure 41) and compared to the experimentally measured profile. The results did not agree, though this is most likely as the Finnie model is known to be inaccurate [6] and requires calibration for specific conditions, which is outside of the scope of this work.

Despite the slight disagreement in particle impact velocity distribution, the trends of the results agreed sufficiently, and the model had been sufficiently validated, to proceed with wear map production.

5.2. Wear Mapping

Wear maps are advantageous compared to conventional methods of modelling erosion as they can be used to accurately predict wear rates for a material in new and complex flow regimes, instead of being limited to describing a specific scenario or giving qualitative ranking of materials [1]. These findings were repeated during the wear map method validation work, detailed fully in Appendix A.1. This increases confidence that the wear maps presented in Figure 12 are valid.

The wear maps were produced by combining the computational model results, Figure 8, with the wear scar profiles measured, Figure 10. These profiles show that the PBF material performed worse than the conventional material, with generally greater wear observed in all scenarios. Unfortunately, repeat experiments could not be performed until a few weeks before the project deadline, and so the post-processing required to gather repeat profiles could not be completed. This is a significant source of error in this report, and this error is carried forwards into lower confidence in the wear maps. However, there are no obvious errors, with general trends corresponding to other wear profiles in the literature [1,2,30].

This report presents wear maps for AM materials and conventionally manufactured materials for the first time. The maps for the PBF material show generally increased wear over their conventional counterparts, and this is a general increase with no significant differences in specific locations. This is likely as the particle tracing model data does not take the incident material into account, so the only difference is the wear profile data. A key simplification made to the model is that the particles freeze on impact; in reality particles are theorised to bounce, and they may regain sufficient speed via acceleration in the flow to contact and remove further material. This bouncing is likely influenced by material properties such as Young's modulus, and this could be observed on a wear map generated with this data.

In contrast to the wear map validation results, when the wear maps were verified by comparing the predicted and actual wear for a 15ms-1 flow velocity, the maps did not perform, with an average MASE of 106%. The maps did reproduce the input data accurately, with an average MASE of 26%, so this is likely not an issue with the map generation code. The greater delta in flow velocity (10ms-1) than in the validation work (5ms-1) is likely the largest contributing factor. This is as the wear maps rely on linear interpolation, which means that predictions for new data will be linearly interpolated from the input data, while the trend observed experimentally is not linear (explain). The accuracy of the maps can be improved significantly by incorporating the 15ms-1 data, with the MASE reducing to 29%, however no unseen experimental data is then available to validate this. These maps are presented in Appendix A.

Chapter 6 – Conclusion

6.1. Conclusions

Erosion, corrosion, and erosion-corrosion performance of conventionally and additively manufactured materials has been investigated by combining the experimental results from a submerged impinging jet apparatus with a corresponding computational model. However, repeat experiments were not completed due to equipment malfunction which has reduced confidence in the final results.

In contrast to Gnanavelu, the wear maps presented were found to unsuccessfully predict wear profiles for the intermediary flow velocity ($15ms^{-1}$), with MASE of 106% compared to 16.7%. This is because linear interpolation limits the useful range of a wear map to conditions close to the calibration data. More work needs to be done with a well calibrated map to investigate if this could then predict wear in a new flow environment; this would allow complex systems to be evaluated in the deign phase.

6.2. Achievements and Impact

- A credible CFD simulation of a SIJ has been developed; comprehensive sensitivity and convergence testing was conducted; and the model was verified and validated by comparison to analytical solutions, previous models, and experimental data.
- Material and condition specific wear maps have been produced for conventionally and AM materials, which, in addition to predicting wear in new conditions, have been compared directly to evaluate differences in performance.
- A unique machine learning (ML) model has been developed which successfully overcomes the limitations of the wear map method, discussed in Appendix B.
- **Impact**: The wear maps and conclusions in this report can be used by Sulzer to predict the wear behaviour in fluid handling components for new AM materials.

6.3. Future work

In future, the computer simulation presented in this report could be extended to model the rebound of particles which would increase the input data to the wear maps, improving their resolution and thus potentially their performance. Rebounds would also be influenced by the material, which may allow further differences between the conventional and AM materials to be observed.

The confidence in the ML model (Appendix B) would improve from further interrogation, including a comparison of different ML architectures; sensitivity and convergence testing; investigation of advanced methods to prevent over fitting such as (momentum); and techniques such as physics guided ML training. This could help lead to a general-purpose erosion-corrosion model which, at this time, remains elusive.

Chapter 7 – References

1. Gnanavelu A, Kapur N, Neville A, Flores JF. An integrated methodology for predicting material wear rates due to erosion. Wear 2009;267:1935–44.

2. Owen J, Ramsey C, Barker R, Neville A. Erosion-corrosion interactions of X65 carbon steel in aqueous CO2 environments. Wear 2018;414–415:376–89.

3. Burson-Thomas CB, Wood RJK. Developments in Erosion–Corrosion Over the Past 10 Years. J Bio Tribocorros 2017;3.

4. Bowman E, Koch G, Varney J, Thompson N, Moghissi O, Gould M, et al. International measures of prevention, application, and economics of corrosion technologies study. Houston: 2016.

5. Laleh M, Hughes AE, Xu W, Gibson I, Tan MY. Unexpected erosion-corrosion behaviour of 316L stainless steel produced by selective laser melting. Corros Sci 2019;155:67–74.

6. Gnanavelu A, Kapur N, Neville A, Flores JF, Ghorbani N. A numerical investigation of a geometry independent integrated method to predict erosion rates in slurry erosion. Wear 2011;271:712–9.

7. Owen J, Godfrey J, Ma W, de Boer G, Al-Khateeb M, Thompson H, et al. An experimental and numerical investigation of CO2 corrosion in a rapid expansion pipe geometry. Corros Sci 2020;165.

8. Coyle D, Hampton L. 21st century progress in computing. Telecomm Policy 2024;48:102649.

9. Fletcher DF. The future of computational fluid dynamics (CFD) simulation in the chemical process industries. Chemical Engineering Research and Design 2022;187:299–305.

10. Leukel J, González J, Riekert M. Adoption of machine learning technology for failure prediction in industrial maintenance: A systematic review. J Manuf Syst2021;61:87–96.

11. Hsu SM, Shen MC, Ruff AW. Wear prediction for metals. Tribology 1997;30:311–83.

12. Redondo C, Chávez–Modena M, Manzanero J, Rubio G, Valero E, Gómez–Álvarez S, et al. CFD–based erosion and corrosion modelling in pipelines using a high–order discontinuous Galerkin multiphase solver. Wear 2021;478–479.

13. Jafar Mazumder MA. Global Impact of Corrosion: Occurrence, Cost and Mitigation. Global Journal of Engineering Sciences 2020;5.

14. Li T. M5080 Individual Report. Leeds: 2024.

15. Thorat U, Jones M, Woollam R, Owen J, Barker R, Thompson H, et al. Computational Fluid Dynamics driven mass transfer model for the prediction of CO2 corrosion in pipelines. Journal of Pipeline Science and Engineering 2023;100148.

16. Finnie I. Erosion of surfaces by solid particles. Wear 1960;3:87–103.

17. Finnie I. Some observations on the erosion of ductile metals. Wear 1971;19:81–90.

18. Blazek J. Chapter 2 - Governing Equations. In: Blazek J, editor. Computational Fluid Dynamics: Principles and Applications (Third Edition). Oxford: Butterworth-Heinemann; 2015. page 7–27.

19. Verhnjak O, Hriberšek M, Steinmann P, Ravnik J. A novel two-way coupling model for Euler-Lagrange simulations of multiphase flow. Eng Anal Bound Elem 2020;119:119–32.

20. Saidi MS, Rismanian M, Monjezi M, Zendehbad M, Fatehiboroujeni S. Comparison between Lagrangian and Eulerian approaches in predicting motion of micron-sized particles in laminar flows. Atmos Environ 2014;89:199–206.

21. McLaury BS. Predicting solid particle erosion resulting from turbulent fluctuations in oilfield geometries. 1996;

22. Franco D, Miller Devós Ganga G, de Santa-Eulalia LA, Godinho Filho M. Consolidated and inconclusive effects of additive manufacturing adoption: A systematic literature review. Comput Ind Eng 2020;148.

23. Chao Q, Cruz V, Thomas S, Birbilis N, Collins P, Taylor A, et al. On the enhanced corrosion resistance of a selective laser melted austenitic stainless steel. Scr Mater 2017;141:94–8.

24. Alderton J. M5080 Individual Report . Leeds: 2024.

25. Maddison J. M5080 Individual Report . Leeds: 2024.

26. Celik IB, Ghia U, Roache PJ, Freitas CJ, Coleman H, Raad PE. Procedure for estimation and reporting of uncertainty due to discretization in CFD applications. Journal of Fluids Engineering, Transactions of the ASME 2008;130:0780011–4.

27. Tu J, Yeoh GH, Liu C. Practical Guidelines for CFD Simulation and Analysis. In: Computational Fluid Dynamics. Elsevier; 2018. page 255–90.

28. Poreh M, Tsuei Y, Cermak JE. Investigation of a turbulent radial wall jet. Applied Mechanics 1967;34:457–66.

29. Hyndman RJ, & AG. The forecaster's toolbox. In: Forecasting: Principles and Practice. Monash University; 2018.

30. Barker R, Hu X, Neville A. Evaluating Inhibitor Performance in CO 2-Saturated, Erosion-Corrosion Environments. Corrosion 2015;71:14–29.

31. Mohan DD, Jawade B, Setlur S, Govindaraju V. Deep metric learning for computer vision: A brief overview. Handbook of Statistics 2023;48:59–79.

32. Alpaydin E. Introduction to Machine Learning. MIT Press; 2010.

33. Alpaydin E. Introduction to Machine Learning. 3rd ed. The MIT Press; 2014.

34. Imran MH, Jamaludin S, Ayob AFM, Ali AAIM, Ahmad SZAS, Akhbar MFA, et al. Application of Artificial Intelligence in Marine Corrosion Prediction and Detection. J Mar Sci Eng2023;11.

35. Ossai CI. A data-driven machine learning approach for corrosion risk assessment—a comparative study. Big Data and Cognitive Computing 2019;3:1–22.

36. Wang Z, Chen H, Wang M, Zhang X, Dou Y. Solid particle erosion prediction in elbows based on machine learning and swarm intelligence algorithm. J Pet Sci Eng 2022;218.

37. Cloutier R, BC, BMA. Systems Engineering Simplified. 1st ed. CRC Press; 2015.

38. Ali O, Abdelbaki W, Shrestha A, Elbasi E, Alryalat MAA, Dwivedi YK. A systematic literature review of artificial intelligence in the healthcare sector: Benefits, challenges, methodologies, and functionalities. Journal of Innovation and Knowledge 2023;8.

39. Tran A, Furlan JM, Pagalthivarthi K V., Visintainer RJ, Wildey T, Wang Y. WearGP: A computationally efficient machine learning framework for local erosive wear predictions via nodal Gaussian processes. Wear 2019;422–423:9–26.

40. Guo X, Li W, Iorio F. Convolutional Neural Networks for Steady Flow Approximation. In: Proceedings of the 22nd ACM SIGKDD International Conference on Knowledge Discovery and Data Mining. New York, NY, USA: Association for Computing Machinery; 2016. page 481–90.

41. Tian HH, Addie GR, Pagalthivarthi K V. Determination of wear coefficients for erosive wear prediction through Coriolis wear testing. In: Wear. 2005. page 160–70.

42. Yang SD, Ali ZA, Kwon H, Wong BM. Predicting Complex Erosion Profiles in Steam Distribution Headers with Convolutional and Recurrent Neural Networks. Ind Eng Chem Res 2022;61:8520–9.

43. Tjøstheim D, Otneim H, Støve B. Regression and conditional regression quantiles. Statistical Modeling Using Local Gaussian Approximation 2022;385–401.

44. Al-Sabaeei AM, Alhussian H, Abdulkadir SJ, Jagadeesh A. Prediction of oil and gas pipeline failures through machine learning approaches: A systematic review. Energy Reports2023;10:1313–38.

Appendix A

A.1. Wear Map method

1.1. Gnanavelu's wear map

The wear map presented by Gnanavelu [1], is adopted from their 2009 journal article published in Wear and is presented here as an example for the reader, and for comparison to the reproduction that follows in subsection 1.2.

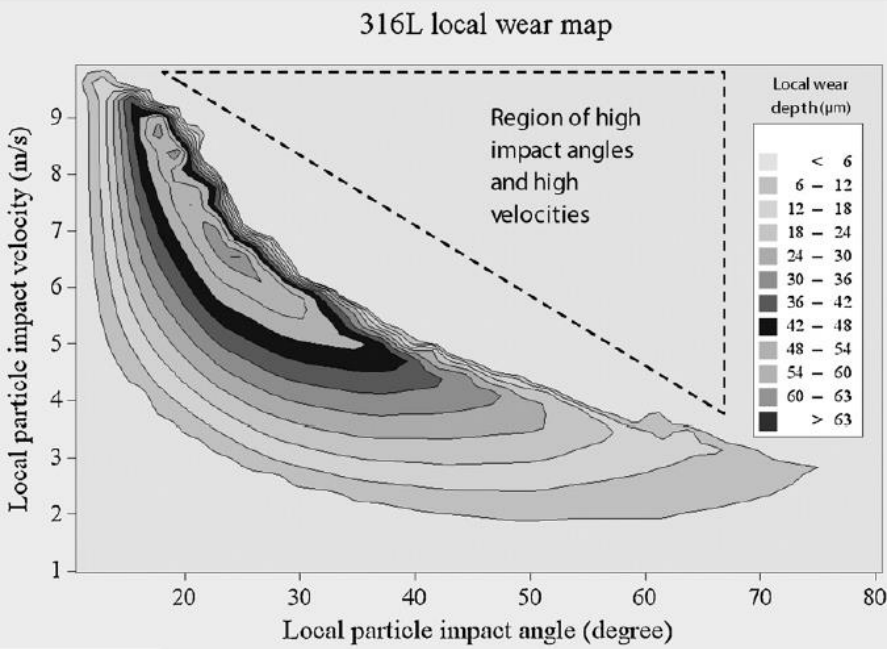

Figure 14 - Wear Map, adopted directly from Gnanavelu [1].

1.2. Reproducing Gnanavelu's wear map [1]

The MATLAB code developed to reproduce a similar map was validated through reproduction of this map. This is discussed in the main report, supporting figures follow.

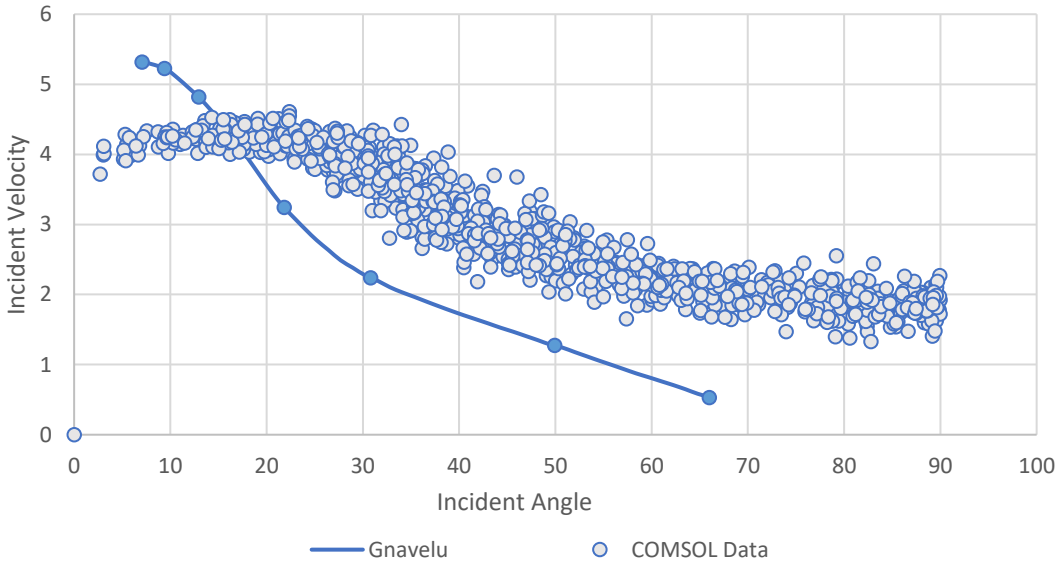

Figure 15 - Particle incident velocity and angle, computed by changing the nozzle diameter to 7mm and the flow velocity to 10ms^{-1} to match Gnanavelu's method [1].

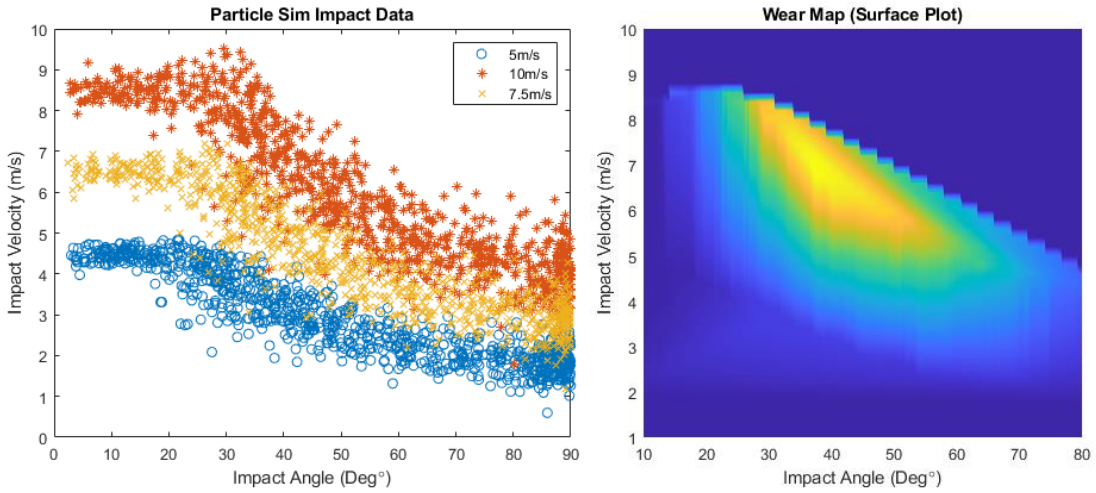

Figure 16, Figure 17 – Complete CFD simulation particle impact results, and the resulting wear map produced using MATLAB. The wear map is comparable to that discussed in subsection 1.1.

1.3. Validating the wear map method

The performance of the map given by Figure 16 is evaluated by testing if the input data can be reproduced (Figure 18) and if the 15ms^{-1} data can be predicted.

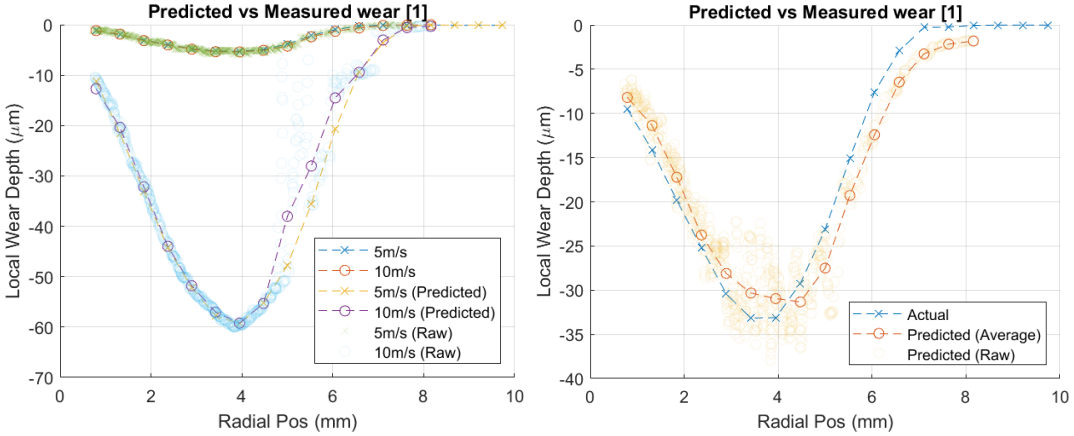

Figure 18, Figure 19 – Validation of wear map performance against the initial, and the test data. Results mirror those of Gnanavelu [1], with the 15ms-1 flow velocity wear profile correctly predicted.

A.2. Mesh Convergence and Sensitivity testing

2.1. Initial Mesh Convergence

Full results for the convergence of the average shear stress at the sample surface are provided in Table 2 for completeness. This initial mesh convergence was done by adapting the simulation geometry such that the analytical results given by Poreh et al. [28] can be used to validate the model.

Table 2 – Initial Mesh convergence results, shear stress at the wall is investigated with the GCI calculated.

Number of Elements	Average Shear Stress (Pa)	% Change	r_{eff}	p_{eff}	GCI
2,565	87.49				
10,260	77.28	13.21%	2.00		
41,040	81.36	-5.02%	2.00	1.32	4.18%
64,125	85.29	-4.61%	1.25	0.17	151.49%
90,375	84.04	1.49%	1.19	6.66	0.87%
130,560	83.82	0.26%	1.20	9.51	0.07%

2.2. Sensitivity Results – Y+

The shear stress and the variation of the y+ distribution at the sample surface is given.

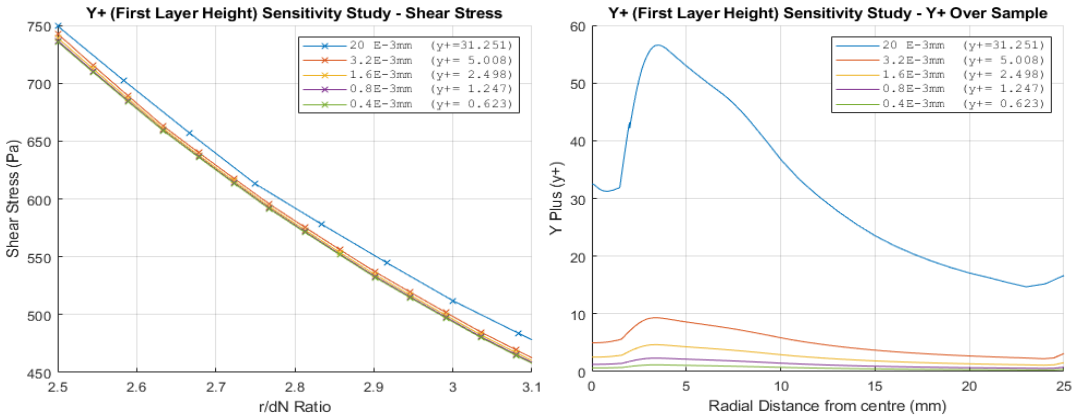

Figure 20, Figure 21 – Wall shear stress convergence with first element height, and the corresponding y+ distribution at the sample surface is presented. Results converge below 0.8E-3mm.

2.3. Particle Size

The particle size specified by the particle tracing module was found to have the greatest influence on the results, with smaller particles computed to show greater variation in impact velocity and angle with radial distance from the nozzle. This is as smaller particles can be more easily accelerated by the impinging flow at nozzle. As discussed, 250μm particles were selected as this is the average of the erodent used, but a model that accounts for the variation in size would be advantageous.

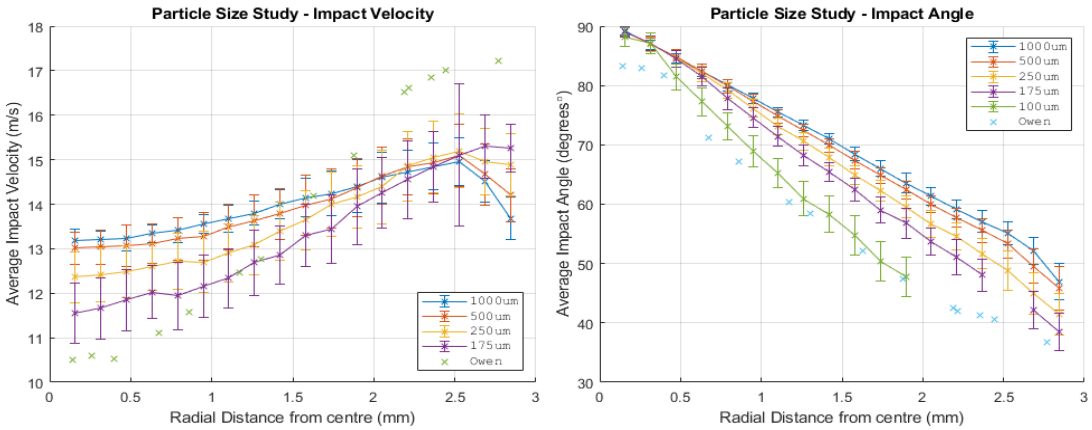

Figure 22, Figure 23 – Influence of particle size on the particle impact velocity and angle distributions.

A.3. Final model supplementary results

3.1. Final mesh convergence

A final mesh convergence study was conducted, with the full results given in Table 3. A 67,840-element mesh was selected, as subsequent refinement does not yield further change in the results (GCI<1%).

Table 3 - Final Mesh Convergence Results, Factor of Safety (FS) for GCI calculations is 1.25 (rigorous).

	Impact Velocity (m/s)		Impact Angle (deg)		Shear Stress (Pa)	
Number of Elements	Average	GCI	Average	GCI	Average	GCI
7,552	13.56		66.74		539.92	
21,136	13.63		66.54		518.66	
67,840	13.64	-0.04%	66.43	0.22%	512.82	0.54%
90720	13.65	-0.01%	66.43	0.00%	515.23	-0.41%
106,000	13.66	0.14%	66.45	0.06%	516.95	-1.06%

3.2. Simulation Graphics

The shear rate and the turbulent kinetic energy at the nozzle are given in Figure 24, illustrated by discrete colour bands. Results are comparable to similar simulations [1,2].

- The shear stress and y+ distributions at the wall, and their variation with the flow velocities simulated, are given in Figure 26.
- Finally, the flow velocity at 15ms^{-1} is presented in Figure 28 for completeness.

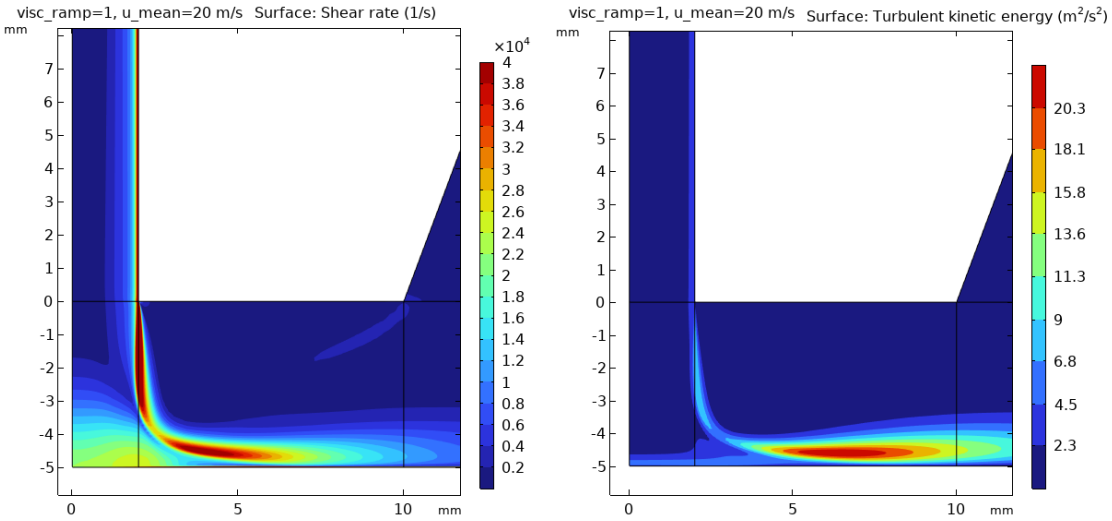

Figure 24, Figure 25 – Final simulation, shear rate and the turbulent kinetic energy at 20ms^{-1}.

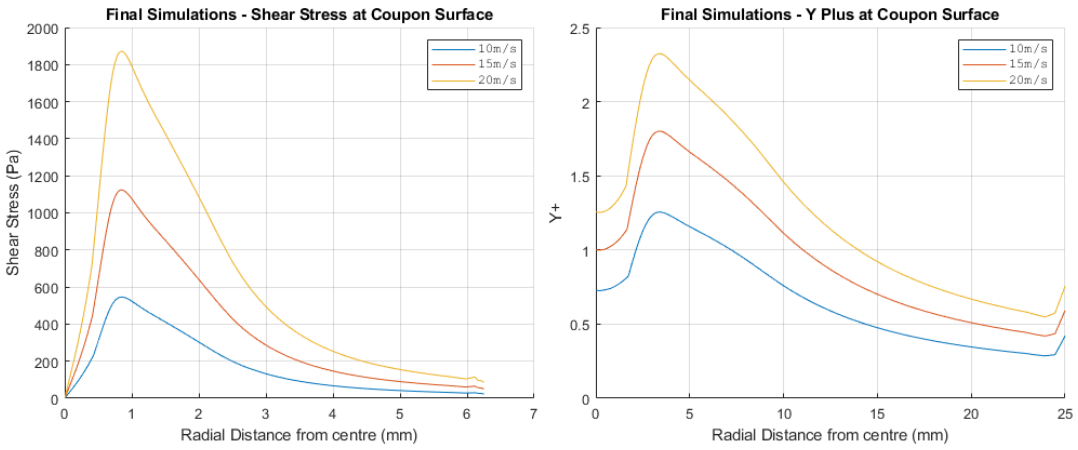

Figure 26, Figure 27 – Final simulation, variation of shear stress and y+ distributions at the wall with $\bar{u}$.

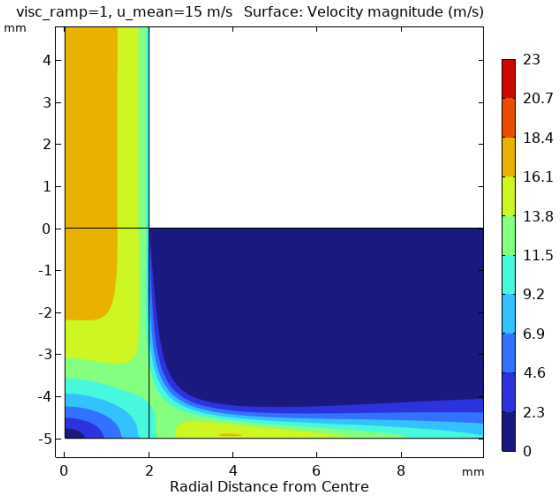

Figure 28 - Final simulation, flow discrete velocity contours at $\bar{u} = 15ms^{-1}$.

3.2. Raw Particle Data

The raw particle data, with comparison to results provided by Owen [2], are given in Figure 29 - 5000 particles are simulated with $\bar{u}$ equal to 10, 15 and 20ms^{-1}.

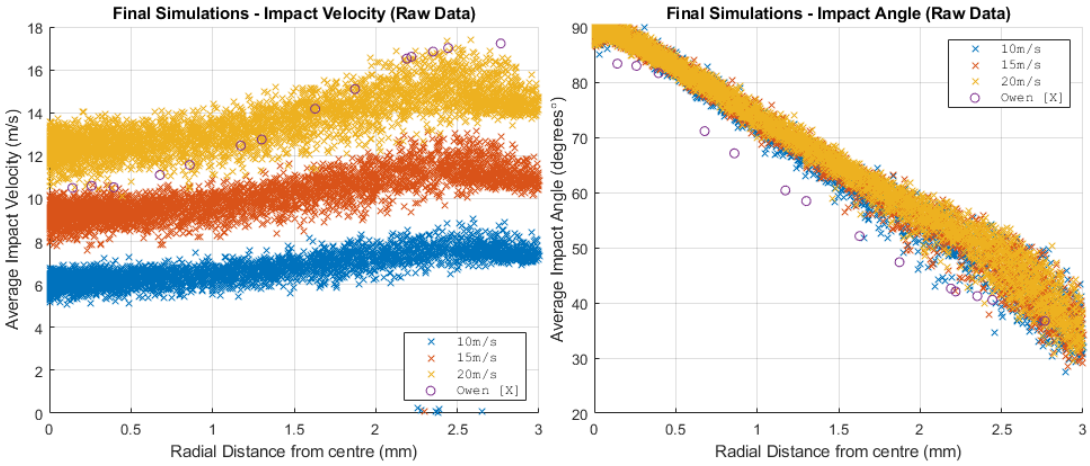

Figure 29, Figure 30 – Final Simulation, raw particle data (5000 particles), and comparison to Owen [2].

A.4. Wear map prediction profiles (15ms^{-1})

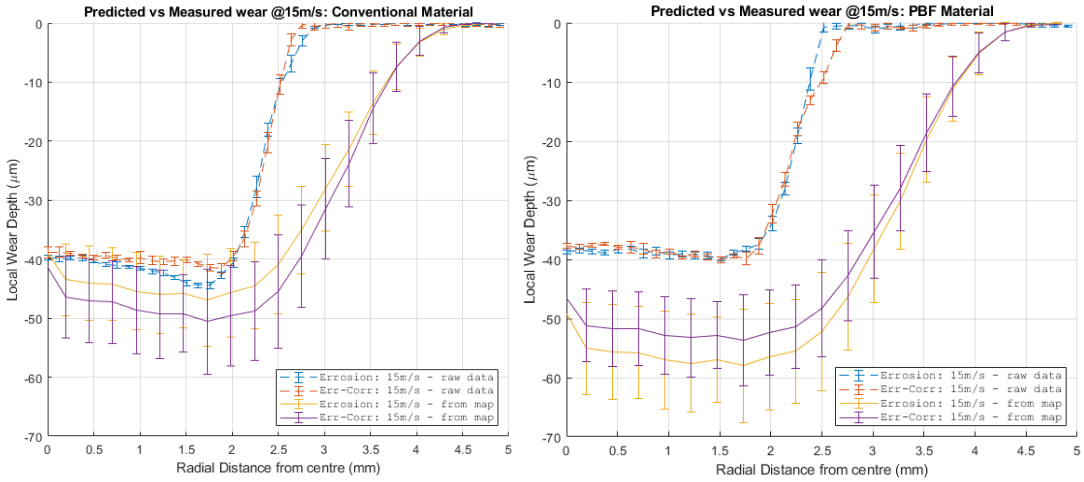

Figure 31, Figure 32 – Wear profile prediction comparison. Map does not predict 15ms^{-1} accurately.

A.5. Miscellaneous

5.1. Additional particle equations

The component forces on an individual particle, eq. 5-7, act on the particle as shown:

$$\frac{d(m_v v)}{dt} = F_t = \sum F_{Drag,\ Buoyancy,\ Gravity} \quad (4)$$

The Schiller-Neumann drag force formulation is used to calculate the drag force coeff.:

$$\beta = \frac{3}{4d_p}\phi_d C_D \rho \left| u_{slip} \right| \quad (5)$$

Buoyancy force is calculated (for a 250μm particle) to be 1.3377e^{-7} N, as follows:

$$F_{Buoyancy} = \frac{1}{6}\pi d_p^3 (\rho_p - \rho) g \quad (6)$$

Gravity force is calculated as:

$$F_{Gravity} = m_p g \frac{\rho_p - \rho}{\rho} \quad (7)$$

5.2. Final CFD Model Geometry and Mesh Details

Figure 33 shows the final CFD geometry and an example 1000 element mesh to illustrate how edge biases were used to control the height of cells at the walls of interest (nozzle and sample) while growing at the fluid domain extremities to improve the computational efficiency of the model. Figure 33 also shows the excellent mesh quality, coloured by the skewness, which is a minimum of 0.7716, and an average of 0.9766. This quality is preserved when the mesh element number is increased.

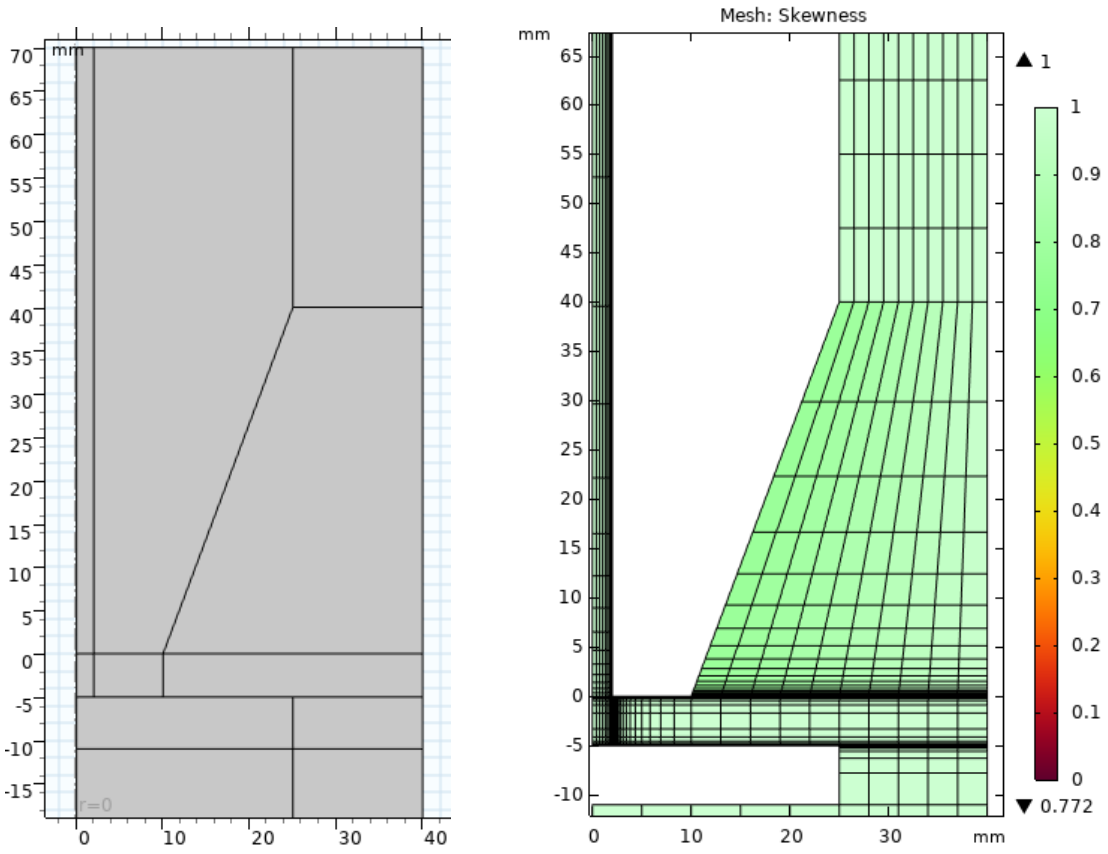

Figure 33, Figure 34 – Final fluid geometry and a coarse mesh to illustrate the meshing strategy.

5.3. Wear Maps built with 15ms^{-1} data.

Add 15ms^{-1} data to improve the predictions from the wear map method. Maps change significantly, as shown between Figure 35 (no 15ms^{-1} data) and Figure 36, built including the 15ms^{-1} data. The map resolution at high impact angles and lower velocities is much improved.

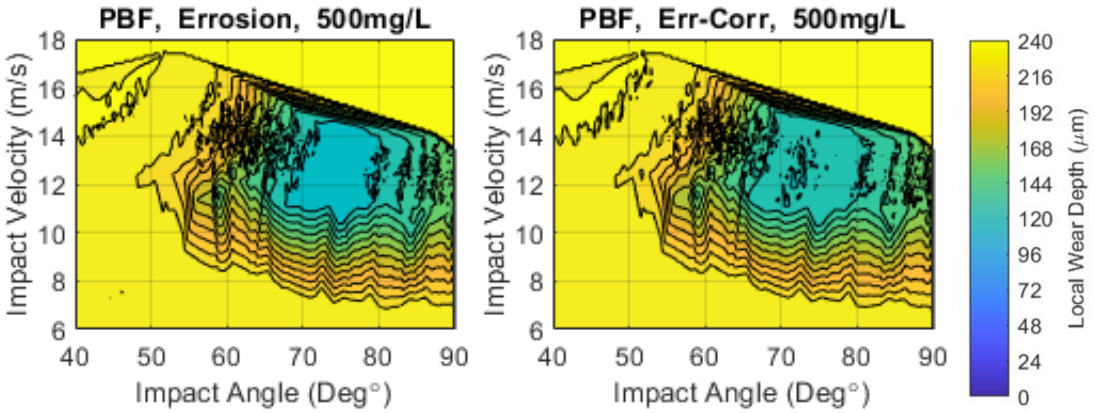

Figure 35 - Select maps, built with no 15ms^{-1} data.

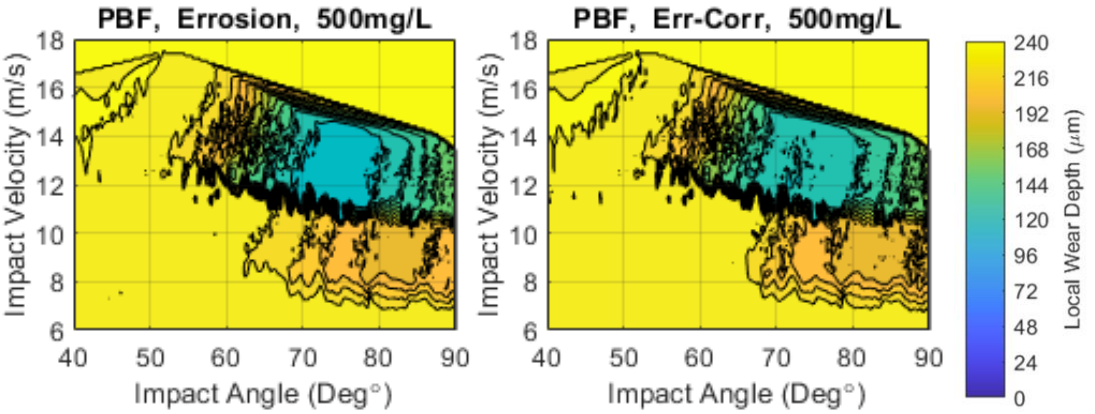

Figure 36 - Select maps, built with 15ms^{-1} data. Resolution is improved.

5.4. Full Resolution Wear Map

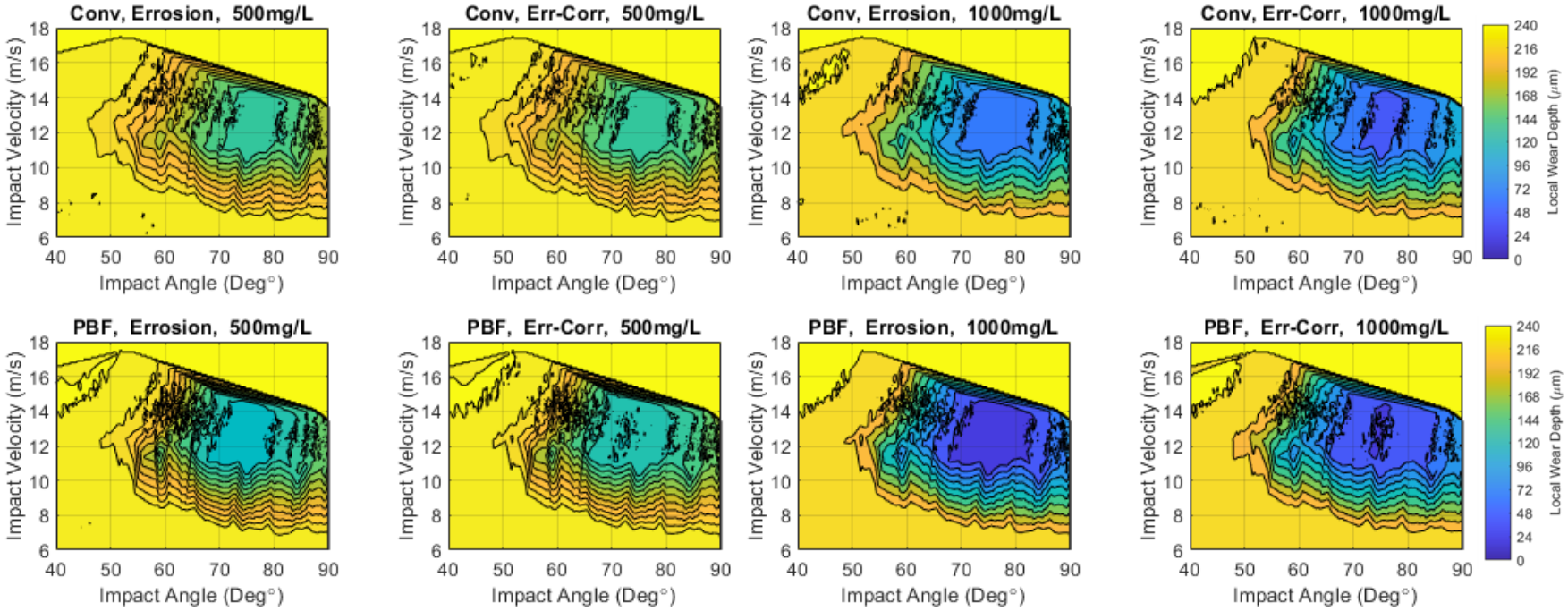

Figure 37 - Full resolution wear maps.

Appendix B

B.1. Introduction

A limitation in our current understanding of erosion and erosion-corrosion is the ability to accurately predict local wear rates, especially in complex conditions [1,3]. Wear maps can be used confidently if the map has been calibrated with experimental results of the material and conditions of interest, though the results of this report indicate that (as this method relies upon linear interpolation) non-linear relationships cannot be accurately described. Traditional approaches, such as those presented by Finnie [16], are founded with a mechanistic understanding of the processes involved but require material and condition specific empirical constants to be useful [3,11]. A different approach is required if a general-purpose model is to be successful.

B.2. Literature Review

Machine learning (ML) has garnered significant public attention in recent years, with the advent of large language models (LLMs), such as Chat GPT, proving the incredible power and potential of the technology [31]. Chat GPT is an example of a generative pre-trained transformer, which is a category of ML models designed to decipher natural language.

Generally, ML algorithms can be divided into supervised and unsupervised learning problems [32,33]; this review will focus on supervised learning which is used to train the classification and regression models of interest. In supervised learning, models are trained by providing input data, X, and corresponding output data, Y, with the aim of finding the path (or mapping) between them. There is no output training data for unsupervised models, the aim is to perform density estimation where the model looks for patterns in the input data.

Supervised models can be divided into classification and regression problems [32,33]. The former output probability distributions of a (fixed) number of categories that a model expects, while the latter can produce continuous responses.

2.1. Classification Problems

Classification models are the most common ML approach as, with our current technology, they generally outperform regression techniques [32]. This is reflected in their popularity. For example, in a systematic review of ML techniques used in industrial failure and maintenance prediction, classification algorithms such as random forest and support vector machines were associated with 94% of the studies evaluated [10].

Marine corrosion is another field where ML technology is used, as discussed in a systematic review by Imran et al. [34]. Many of these models do not predict corrosion from analytical data exclusively, however, which means they cannot be used preventatively in the design phase. Instead, the most common ML approach reviewed by the authors, are those which inspect real-time data of an operational system that is gathered non destructively, for example, via computer vision, electromagnetic or acoustic techniques. The models analyse experimental data to predict the probability of failure, sometimes in combination with a conventional statistical model.

An example of an analytical model that Imran et al. discuss is a data-driven machine learning approach for corrosion risk assessment [35]. The author, Ossai C., presents a deep learning neural network (DNN) that evaluates the expected corrosion defect depth in pipelines from data such as the temperature, CO2 partial pressure and ion concentrations. This approach yielded improved accuracy over other models, though a key limitation of the study is that the local corrosion rate is not calculated, and no system specific geometry is considered. The influence of erosion is also not considered, which is a key consideration in slurry transport where erosion and erosion enhanced corrosion are significant [1].

Erosion rate has been predicted analytically, as presented by Wang et al. in a study on pipe elbows, who use a ML model that accepts experimental data such as the pipe material, diameter, curve radius and particle diameter [36]. The model could predict the maximum erosion rate expected in the elbow with a high degree of accuracy (RMSE=0.82e-3) [36], and the model could describe the trends expected from dimensionless input data.

Though these models can be more accurate than conventional statistical models, if the local wear rate can be predicted empirically, and earlier in a design phase, costs may be reduced significantly. This is because during the development of a system, in general, around 70% of the total cost to develop it is committed [37]. Improving the understanding of a systems performance will allow more effective countermeasures and maintenance plans to be put in place, reducing lifecycle costs.

2.2. Regression Models

Regression models are generally less successful that classification models [32], though, they have been successfully adopted in several fields, including in healthcare systems [38] and, most relevantly, in industrial failure prediction [10]. The main advantage is that a continuous response can be generated, which would be vital in predicting local erosion rates.

Unlike classification models, which place input data, X, into discrete categories, Y, regression models attempt to fit a function to map the X and Y data [32]. In the most basic case, this could be a linear function ($y = mx + c$) fit to some input data where the model looks to reduce the fitting error by optimising some parameters (m, c), or more params for a higher order function (e.g., for polynomial $y = m_2x^2 + m_1x + c$, m_2, m_1, c).

An example of a successful regression model, named WearGP, is presented by Tran et al. [39]. The author's aim was to reduce the computational resources required to predict wear rates by developing an artificial neural network (ANN) that uses a nodal gaussian process. This work follows from previous research into ML models that can predict CFD flow solutions [39], such as the convolutional neural network proposed by Guo et al. to approximate steady flows [40]. WearGP was trained with CFD simulation data and the corresponding nodal wear solutions of slurry pump impellers. They obtained accurate results of local wear rates, comparable with those obtained via CFD, with a 10^6 order reduction in computational time.

It is important to note that the impeller wear data the model was trained with was not gathered from experimental testing. Instead, data from Coriolis wear testing [41] was synthesised with the CFD predicted flow and particle results to predict a wear rate at each node. Therefore, it is difficult to determine if this wear model will produce valid results for determination of wear in different scenarios. The model also only predicts erosive wear and does not consider corrosion.

A similar approach was used by Yang et al. who predict complex erosion profiles in steam distribution headers [42]. Their model again predicts particle trajectories and erosion profiles accurately, though it is unlikely that these models can produce useful predictions for a different application, and corrosion is not considered.

While these authors prove that significant time is saved once an accurate model is produced, a large amount of data and time is required to build and prove the model is accurate for the conditions of interest. This is worthwhile if many similar designs could then be evaluated quickly but would not be advantageous for low volume analysis of highly specialised systems. A general ML model would, however, be of interest to a range of industries.

2.3. Evolution of wear map method.

The wear map method, discussed in detail in this report, is limited to predicting linear relationships. This problem is exposed in the results presented in this report, where the map could not predict the wear for a $15ms^{-1}$ flow. The hypothesis of this appendix is that augmentation of this method with a ML regression model may produce a "map" which is not restricted to linearly interpolating from the input data supplied.

A ML model could also accept more input variables than the 2D wear map method. As stated by Hsu et al., there are at least 30 variables of significance to erosion-corrosion performance, such as material hardness [11]. These parameters could be incorporated into a ML model to overcome the material and condition specificity of the wear map method.

Extending this further, the continuous results from physically based models, such as those presented by Finnie [16,17], could also be incorporated. Once a CFD model of a flow has been developed, predicted erosion and corrosion rates at the surface can be calculated without significantly more effort. This information could supplement particle impact data and be used by one model to predict wear in erosion, corrosion, and erosion-corrosion conditions, i.e., a universal wear model.

This approach is fundamentally different to that of "WearGP" proposed by Tran et al. [39], as it would still require a CFD solution to be computed to provide the relevant input data. This would require more time than WearGP, which estimates wear from geometry nodes and boundary conditions only – a significant disadvantage.

However, with CFD used routinely by many industries at the design phase [REF], and with continued rapid progress in computing power [8], the labour and costs to produce a CFD solution would be significantly outweighed by the savings in experimental calibration work, if a universal model can be found.

2.4. Curse of multidimensionality

Theoretically, a large number of parameters and analytical results could be used by a ML model to predict wear, from material properties, flow condition, species transport and timeseries data. However, as discussed by Tjøstheim [43], as the number of dimensions increases, a disproportionally large number of inputs are required.

Therefore, the designer of such a model would need to be selective about which data is most likely to be useful to predict wear, and therefore should be the variables with the strongest correlation. Though this should also be balanced against the data that can feasibly be collected analytically, as the time to collect, verify and validate the input data must be considered against the time to conduct experimental testing.

2.5. Conclusion

Proven by increasing adoption by industry [10,44], and examples such as "WearGP" [39,42], a regression-based ML model could be used to produce a multidimensional space that can accurately predict erosion-corrosion wear. A ML model may be able to overcome the material, condition, and linear relationship limitations of the 2D wear map method presented previously.

B.3. Methodology

To develop a ML model, an architecture must be defined. The model type, the model inputs and the model outputs must be determined. Next, the model must be designed, and the training and testing data defined. Training can then take place, with the success of the model validated against the training data.

3.1. Model Architecture

Though several ML approaches have been discussed, a standard deep neural network was selected because it is easy to implement, and because similar (though more refined) CNNs and ANNs have been shown to perform well [39,42]. A simplified, single hidden layer NN is illustrated in Figure 38.

The final deep neural network consists of many hidden and connected layers, and the final structure selected is given in Figure 39. It should be noted that some trial and error took place to determine the layer order, count, and properties; in future, a structured process that quantifies these choices may yield a model with better performance. This work is presented as a proof of concept.

As with the wear map method, the particle impact angle and velocity are two primary inputs, and the wear depth predicted is the desired output. As discussed in the literature review, a regression model will be required to allow the wear expected to be a continuous variable.

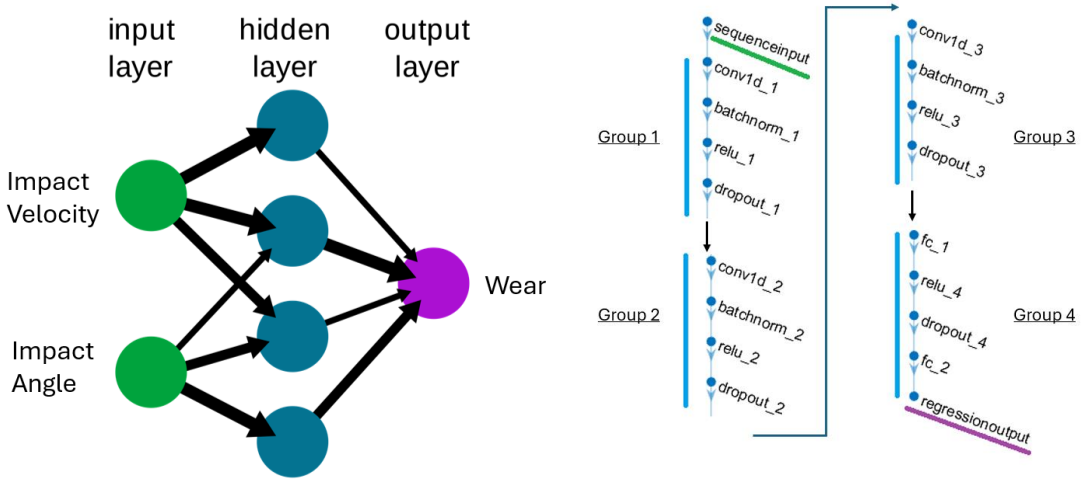

Figure 38 - Simplified NN architecture with 2 inputs, one hidden fully connected layer, and one output.
Figure 39 - Final NN architecture: three hidden layer groups; one fully connected layer with regression.

MATLAB is a versatile tool that has been used throughout the report to read, transform, and compute data. It also provides a suite of tools as part of the “Deep learning toolbox” that were used to quickly develop a model and take advantage of the wear profile and CFD data that was available from the main report.

3.2. Model Inputs

As discussed in the literature review, an advantage of a ML model is that many inputs can be accepted, but that the designer of a model must be selective and restrict the number of inputs to those that are most likely to have the largest impact. This is because the “curse of dimensionality” increases the amount of training data disproportionately with the number of inputs [43]. It also takes significant time to collect and verify additional data, which is a secondary consideration.

The inputs are divided into local and general inputs. General inputs will have the same value for a number of local sample points, corresponding to a condition or material that does not change over the surface. Local inputs vary with the system geometry and are obtained by extending the CFD flow model.

1. Local: Particle impact velocity – from CFD model
2. Local: Particle impact angle – from CFD model
3. General: Material hardness – from material properties or hardness testing
4. General: Condition (Erosion or Erosion-Corrosion)
5. General: Erodent concentration
6. Local: Erosion rate – Finnie model prediction [16] from CFD
7. Local: Mass Transfer Coefficient

The Finnie model [16] erosion rate was selected as it is easily computed from the particle data and is a physically guided quantity that can be interpreted by the model.

The Mass Transfer Coefficient is also obtained analytically. The data for this was obtained from Tsun Li, [14], who extended the CFD model given in this report with a k- ω SST solution, and a model to predict the H^+ ion flux at the sample surface. This was selected as an input as it can be used by the model to adjust the prediction.

Unlike the wear map method, where maps are material and condition specific, these inputs allow one NN to differentiate between all experimental test cases.

3.3. Model Layers

The model layer structure, given in Figure 39, and training options were determined following guides on the MATLAB website, trial and error, and informed from theory [33].

Table 4 - Layer Types and Descriptions, see miscellaneous appendix for code with all layer settings.

Layer Type	**Description**
`sequenceInputLayer`	Accept (7) inputs, and normalise data
`convolution1dLayer`	Apply sliding 1-D filters, dot product weights, add biases
`batchNormalizationLayer`	Normalise each channel independently prior to reluLayer
`reluLayer`	If input is less than zero, set equal to zero
`dropoutLayer`	Set to zero, random probability threshold, helps overfitting
`fullyConnectedLayer (fc)`	Multiply input vector by weights and add a bias
`regressionLayer (output)`	Regression output layer, produces a continuous result

3.4. Training the Model

The following training options, found through trial and error, were used. Settings are likely suboptimal; a design of experiment would allow the effect of these on accuracy to be classified.

```
MaxEpochs=100                % Low to help prevent overfitting
GradientThreshold=1          % Determines the gradient required per iteration
InitialLearnRate=0.002       % Determines the gradient descent speed
ValidationFrequency=5        % Calculate error to training data after 5 itrs.
MiniBatchSize=5000           % 5000 points per training set
```

The ML model is initialised with random weights and biases. Simply, training allows the ML algorithm to compute the error and then perform gradient descent. This process gradually optimises the weights and biases of the model.

The training data selected was all the wear profiles and analytically computed results for the $10ms^{-1}$ and $20ms^{-1}$ data sets only. As with the wear maps, the data from the $15ms^{-1}$ flow velocity experiments and analysis were used as testing data only.

The inbuilt MATLAB training monitor was used to view the model's evolution. The output for the final model presented is given in Figure 40. The blue training line shows the RMSE of the model as training progresses. The error slowly reduces until the maximum iterations (epochs) are completed.

The testing data is used to produce the validation line given in Figure 40. We can see that the RMSE starts fairly low (28) and reduces but then increases at the final iteration. The "final" point marked is the best model configuration selected at the end.

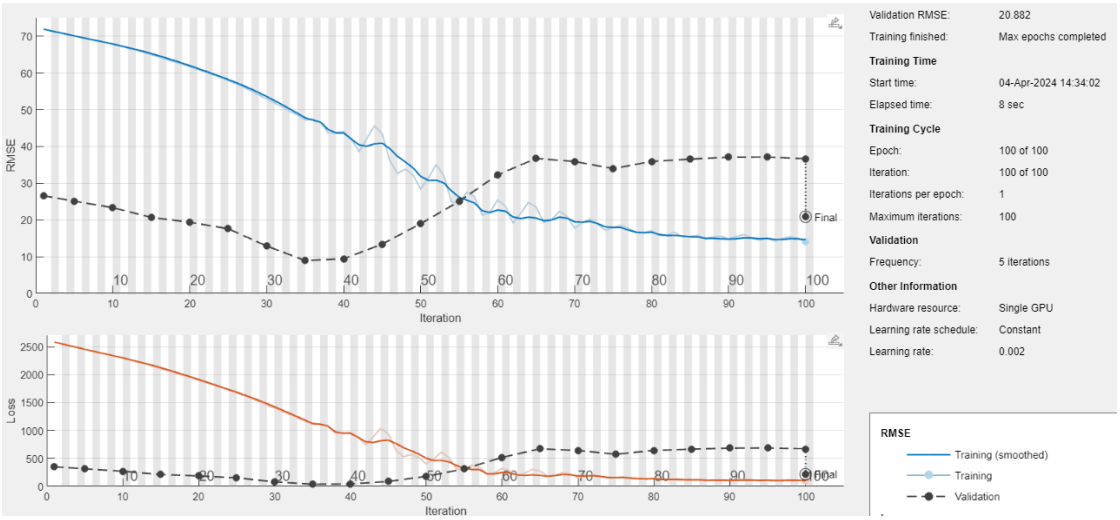

Figure 40 – Final ML model training progress, MATLAB training monitor view. RMSE and Loss given.

A high dropout rate was used to prevent overfitting. This means that the model had to be trained several times; the best performing model was selected as the final result.

B.4. Results

4.1 ML Input Data.

The erosion rate predicted by the Finnie model [16] was computed for each relevant flow scenario in CFD and is presented in Figure 41. Note that the erosion rate in is sampled at regular intervals for interpretability, however, the rate was sampled 5000 times such that for each particle data point, there was a corresponding ER.

The MTFC for the 10,15 and 20ms^{-1} flow scenarios are presented in Figure 41, adopted from Tsun Li's project work [14]. This model predicts the same ion flux at the surface independent of material and erodent rate, so for these cases the same MTFC inputs are used.

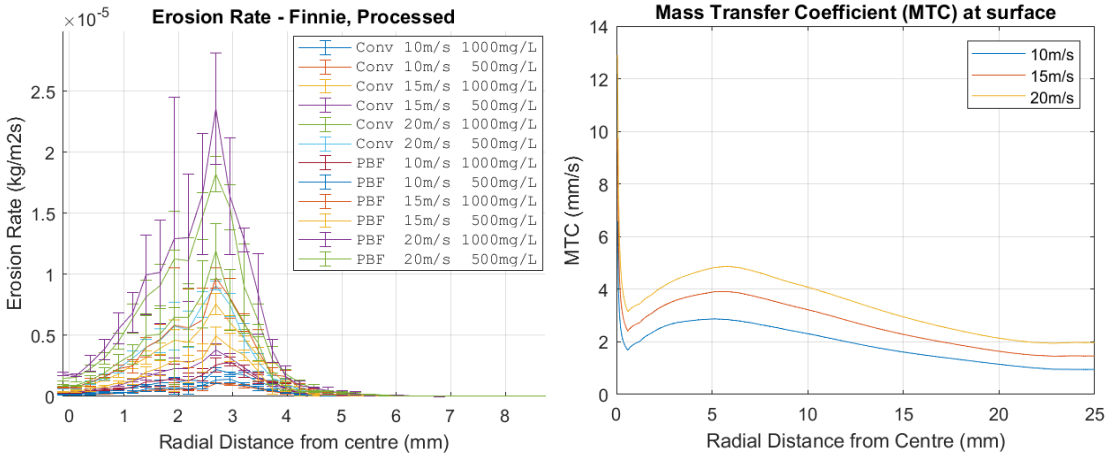

Figure 41, Figure 42 - Erosion Rate predicted (Finnie [16]), and the MTFC adopted from Tsun Li [14].

4.2. ML Predictions

The error for each test case is given for the wear map and ML methods in Figure 43.

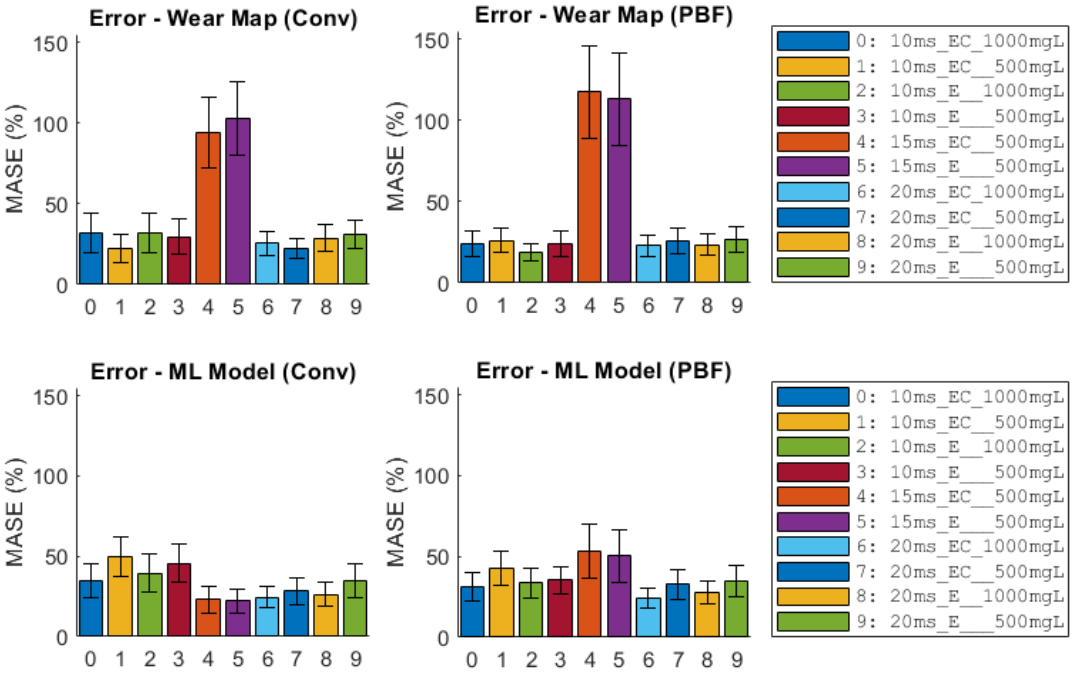

Figure 43 - Results for the ML model compared to the wear map model. MASE: Lower is better.

An example of the prediction for a conventional and PBF material with a 500mg/L erodent flow rate and 15ms^{-1} nozzle flow velocity is given in Figure 44. The ML model outperforms the wear map method, and the confidence in the prediction is greater.

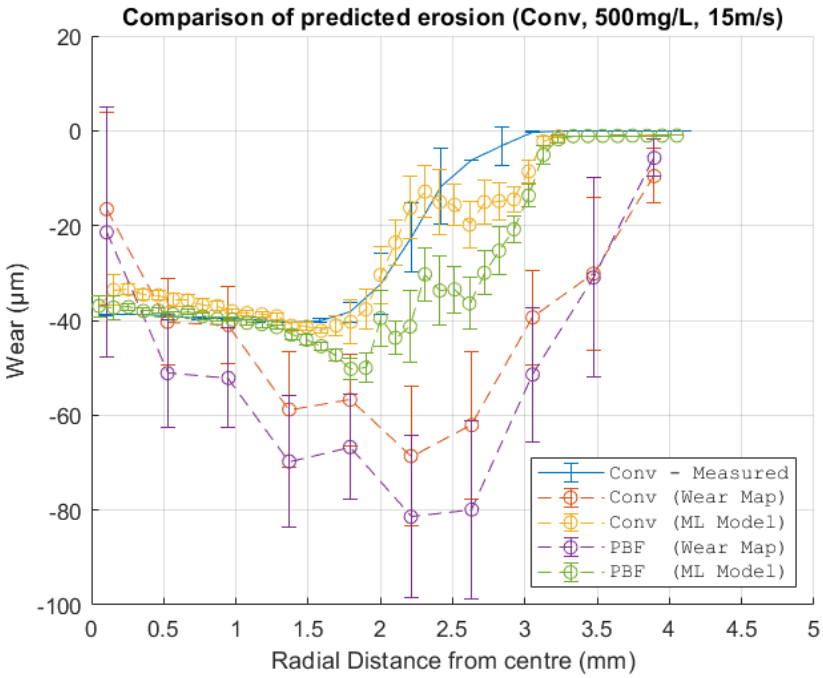

Figure 44 - Comparison between ML and wear map method local wear predictions. A figure with all of the predictions for all test cases is available in section B.7.

4.3. ML Map

We can also compare the wear maps for the ML and wear map methods. Note however that the ML map is produced with only a regular incident angle and velocity grid; no erosion rate or MTFC data is provided, so these maps are limited visualisations.

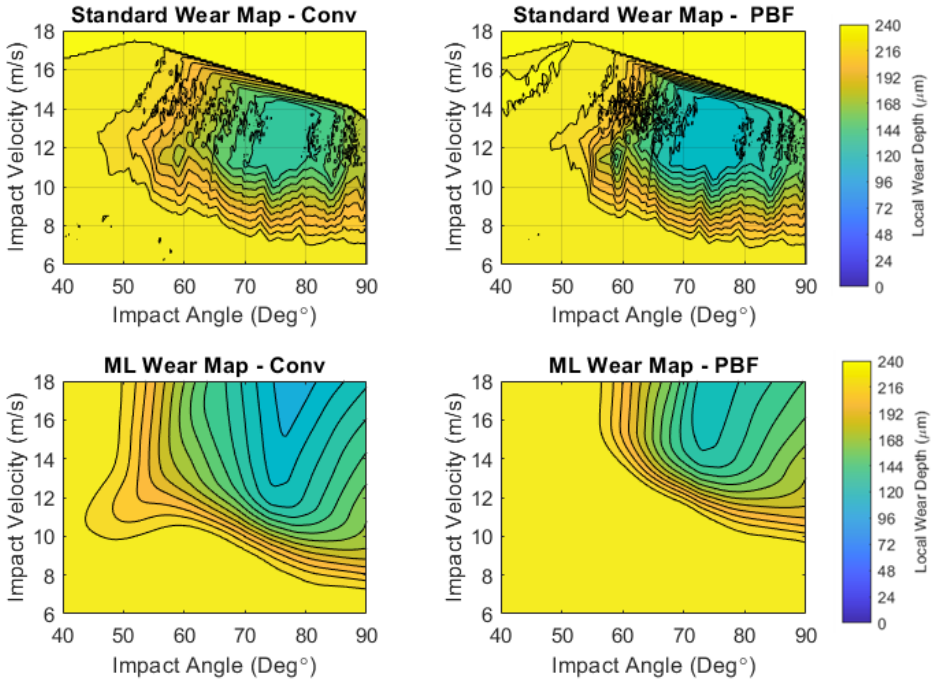

Figure 45 - Wear map comparison between the standard method and the ML model visualisation.

B.5. Discussion

The ML model presented in this Appendix is shown to outperform the wear map method by providing accurate predictions for conditions outside of the training data provided. The wear map method was unable to predict the wear expected for an intermediary 15ms^{-1} flow, with a MASE of 106%, while the ML model predicts the wear scar with an average 37% MASE. This represents a 3x improvement in prediction accuracy, and this is illustrated by the wear scars given in Figure 44.

The ML model reproduces the training data with an average MASE of 34%, which is slightly worse than the wear map method, which reproduces the data used to build the map with a MASE of 26%. However, several maps are required to cover the test space, as they are material and condition specific. The performance of the ML model is impressive as one model can produce results for a range of materials and test conditions.

The maps presented in Figure 45 show significant differences, with the ML maps being smooth and predicting wear for high velocity and high impact angles (which are unlikely due to stagnation regions that slow the flow down). There is also a significant difference between the conventional and PBF ML map, with the higher wear area of the PBF map reduced. However, these maps are just visualisations, and not representative of the underlying ML model, so must treated with caution.

5.1. Limitations and Future Work

More verification work is required to determine if the ML model and methodology presented here is transferable to entirely different flow conditions. This is a key question to verify that this ML model can be applied generally, and could be done, for example, by first testing similar materials and conditions with a new flow regime, such as a rapid pipe expanding geometry [7], and then testing with new materials (with different hardness).

If this model can be shown to perform well, then further research could be done to build on this methodology to produce a general wear model. Some key limitations of the ML architecture presented here is that the erosion-corrosion resistance of the material, the erodent size and hardness, and the corrosive species type are not considered. Also, the wear is predicted for a 3hr test, a general model would need to be non-dimensional, or output an erosion rate from which a depth could be extrapolated.

More advanced ML model architectures could also be employed, such as convolutional and adversarial neural networks [39,42]. Techniques to prevent overfitting should also be considered to reduce the number of training attempts needed.

B.6. Conclusion

A novel deep neural network has been presented that can accurately predict erosion and corrosion wear for both conventional and additively manufactured materials in a variety of conditions. Though the model has several limitations that restrict its employment as a general wear prediction tool, the underlying methodology has been proven to show merit over conventional prediction methods, and suggestions for further research have been presented. These include adopting more advanced ML architectures, such as ANN and CNNs, refining the input choice to consider a wider range of erodent, materials, and conditions.

B.7. Miscellaneous

The wear scars predicted by the ML model and standard wear map method are presented in Figure 46 for completeness.

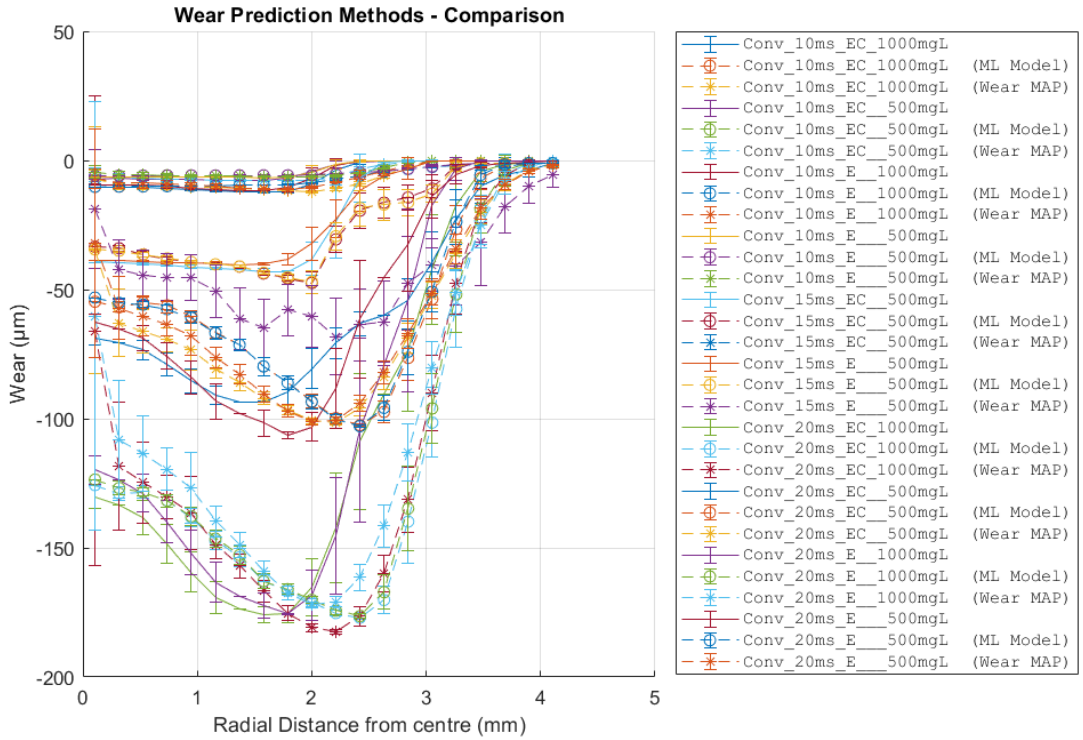

Figure 46 - All wear scar predictions from the ML and wear map methods.